1977

Mercury intrusion porosimetry theory and its application to air-entrained cement pastes and mortars

Ömer Ziya Cebeci
Iowa State University

INFORMATION TO USERS

This material was produced from a microfilm copy of the original document. While the most advanced technological means to photograph and reproduce this document have been used, the quality is heavily dependent upon the quality of the original submitted.

The following explanation of techniques is provided to help you understand markings or patterns which may appear on this reproduction.

1. The sign or "target" for pages apparently lacking from the document photographed is "Missing Page(s)". If it was possible to obtain the missing page(s) or section, they are spliced into the film along with adjacent pages. This may have necessitated cutting thru an image and duplicating adjacent pages to insure you complete continuity.

2. When an image on the film is obliterated with a large round black mark, it is an indication that the photographer suspected that the copy may have moved during exposure and thus cause a blurred image. You will find a good image of the page in the adjacent frame.

3. When a map, drawing or chart, etc., was part of the material being photographed the photographer followed a definite method in "sectioning" the material. It is customary to begin photoing at the upper left hand corner of a large sheet and to continue photoing from left to right in equal sections with a small overlap. If necessary, sectioning is continued again — beginning below the first row and continuing on until complete.

4. The majority of users indicate that the textual content is of greatest value, however, a somewhat higher quality reproduction could be made from "photographs" if essential to the understanding of the dissertation. Silver prints of "photographs" may be ordered at additional charge by writing the Order Department, giving the catalog number, title, author and specific pages you wish reproduced.

5. PLEASE NOTE: Some pages may have indistinct print. Filmed as received.

University Microfilms International
300 North Zeeb Road
Ann Arbor, Michigan 48106 USA
St. John's Road, Tyler's Green
High Wycombe, Bucks, England HP10 8HR

Mercury intrusion porosimetry theory and its application to air-entrained cement pastes and mortars

by

Ömer Ziya Cebeci

A Dissertation Submitted to the
Graduate Faculty in Partial Fulfillment of
The Requirements for the Degree of
DOCTOR OF PHILOSOPHY

Department: Civil Engineering
Major: Soil Engineering

Approved:

Signature was redacted for privacy.

In Charge of Major Work

Signature was redacted for privacy.

For the Major Department

Signature was redacted for privacy.

For the Graduate College

Iowa State University
Ames, Iowa

1977

TABLE OF CONTENTS

INTRODUCTION

The microstructure of an engineering material must be investigated in order to understand its macrostructure and properties, and predict its macrobehavior. The determination of the pore-size distribution of a porous material is an important step in the investigation of its microstructure. Various methods can be employed for pore size analyses, however, every method has some limitations along with its advantages. Evaluation and interpretation of data are usually complicated, because the pore geometry of samples deviates from the ideal models assumed in converting the experimental results to a pore-size distribution curve.

Mercury intrusion porosimetry is one of the latest developed techniques available for pore size analysis. Due to its simplicity and versatility, it has been employed in the determination of the pore-size distribution curves of a wide variety of porous materials (25). This technique is based on the simple phenomenon of the capillary depression of mercury; however, the main disadvantage in applying this principle is the oversimplification of the complex pore geometry of most materials. Various models and different methods of interpretation have been proposed so that a realistic picture of the pore structure of samples can be obtained by mercury intrusion porosimetry.

A clear picture of the microstructure of hardened cement paste is necessary in understanding the structure and properties of concrete. The behavior of concrete can be predicted and controlled if the structure of the paste is known, since hardened cement paste acts as the binding medium in concrete. Hardened cement paste is known to be a porous material (22).

Various techniques, including mercury intrusion porosimetry, have been used by many investigators to determine the pore-size distributions of hardened cement pastes (2,3,9,22,26,27,33).

The purpose of this investigation is to study the physical chemistry of the intrusion and withdrawal of mercury from various pore shapes in order to determine the effect of pore geometry in pore-size distribution curves. New techniques can be investigated and methods developed, so that the interpretation of mercury intrusion porosimetry data can provide more information about the pore structure of materials. The results can be applied to analyze the pore structure of air-entrained cement pastes and mortars. The water-cement ratio of hardened concrete may be estimated by the improved technique. The investigation of these problems by the application of the improved mercury intrusion porosimetry technique is also within the scope of this study.

THEORY

Basic Equations

Washburn, in 1921, proposed determining the pore-size distribution of a porous material by intruding mercury into the pores, stating that, "The pressure required to force mercury into a capillary pore of radius, r, is $-2\gamma\cos\theta/r$, where γ is the surface tension and θ the angle of contact" (30). Very simply, this method involves evacuating the gases from the pores and then forcing mercury into the material by systematically increasing the pressure on mercury. Both the volume of mercury intruded and the pressure to achieve the intrusion are measured. From these data, it is possible to plot cumulative pore volume versus pore radius, thereby producing a pore-size distribution curve. This method assumes that all the pores are cylinders of uniform radius and neglects the fact that they are irregular in shape and may be composed of large cavities interconnected by smaller necks. The pores with necks are referred to as "ink-bottle" pores.

Ritter and Drake (24), in 1945, derived Washburn equation based on the phenomenon of capillary depression, and pointed out that the assumption of cylindrical pore geometry is an important source of error. They published experimental data obtained by mercury intrusion porosimeter on typical porous materials such as activated clays and silica-alumina gels. Ritter and Drake reported that the de-pressurization curve does not coincide with the pressurization curve. This was attributed to mercury being trapped in the ink-bottle pores of the samples.

The assumption of cylindrical pore geometry is far from real especially in the case of a porous material composed of roughly spherical nonporous particles. Therefore, a model of a packing of uniform spheres was adopted by some authors. Kruyer (16) published a theoretical study on such an ideal model where he compared the intrusion of mercury with capillary condensation in the cavities between uniform spheres. Relating the intrusion pressure to the pore size by considering the surface free energies involved, Frevel and Kressley (14) achieved a more general relationship than Washburn equation. They also formulated the relationship between the breakthrough pressure and particle radius for a packing of spheres. By establishing the energy balance involved, Mayer and Stowe (19,20) arrived at the most comprehensive equation relating the intrusion pressure to the change in the interfacial surface areas and in the volume of mercury intruded:

$$P = \frac{\gamma_{l,v}(dS_{l,v}+dS_{s,v}\cos\theta)}{dV} \qquad \text{(Eq. 1)}$$

where P, V, γ and S are terms referring to pressure differential, volume, surface free energy, and surface area, respectively and the subscripts l, s and v refer to liquid, solid and vapor respectively. Equation 1 simplifies to Washburn equation when applied to an opening of a circular cross-section. Mayer and Stowe solved Equation 1 for the intrusion of nonwetting fluids into the void space of a collection of uniform solid spheres and filling of the toroidal void space following initial breakthrough (20).

Recently, DeWit and Scholten (10) assumed that during intrusion, the change in $S_{l,s}$ and $S_{s,v}$ is much greater than the change in $S_{l,v}$ corre-

sponding to the change of the surface area of the mercury meniscus; therefore, $dS_{l,v}$ in Equation 1 may be neglected. If the pores are uniform in cross-section throughout the total length, as in the case of a cylinder or a regular prism, $dS_{l,v}$ is actually equal to zero. However, in the case of tapering cross-sections such as toroidal or conical pores, the change in the surface area of the advancing mercury meniscus may not be negligible. The error caused by this assumption in case of toroidal pore shapes can be calculated by referring to the computations made by Mayer and Stowe as the solution of Equation 1. When $dS_{l,v}$ term is neglected, the values of reduced pressure, i.e., $P/\gamma_{l,v}$, become greater than those tabulated by Mayer and Stowe (20). The error increases to a few hundred percent as the contact angle decreases and the pore size increases.

Intrusion of Conical and Spherical Pores

Most porous materials do not contain cylindrical pores as assumed by Washburn, nor do they consist of a packing of uniform spherical particles as assumed by Mayer and Stowe and others. Conical pore geometry is more realistic than the above models; therefore, Equation 1 is solved here for the intrusion of mercury into a right circular cone. The perpendicular height is h, the radius of the base is r_1, and the radius at the cross-section intruded by mercury is r, shown in Figure 1 as the lines AE, EF and CG, respectively. The side of the cone makes an angle of α with the base. The mercury meniscus represented by GBH is considered as a segment of a sphere with radius R, and forms a contact angle of θ represented as the angle FGJ where the line IJ is the tangent to the segment at its

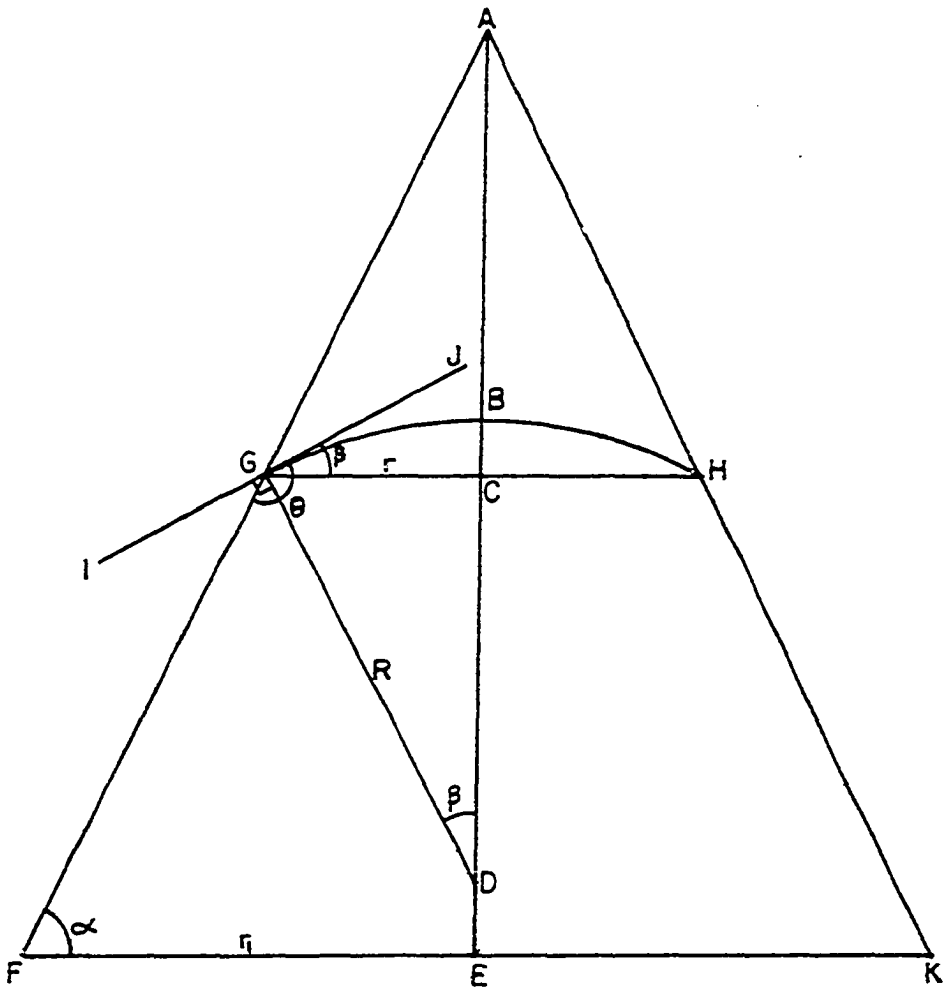

Figure 1. Intrusion of a conical pore

intersection with the cone. For convenience, the angle CGJ or CDG is called β, which is equal to $\theta+\alpha-180$ degrees. Hence, at any stage of intrusion:

$$r = R \sin \beta \qquad \text{(Eq. 2)}$$

The interfacial surface where the solid and vapor phases are in contact is the side of the unintruded part of the cone. Therefore:

$$S_{s,v} = S_{cone} = \pi r\sqrt{r^2+h^2} = \frac{\pi r^2}{\cos\alpha} \qquad \text{(Eq. 3)}$$

and,

$$dS_{s,v} = \frac{d}{dr}\left(\frac{\pi r^2}{\cos\alpha}\right) dr = \frac{2\pi r}{\cos\alpha} dr \qquad \text{(Eq. 4)}$$

The liquid-vapor interface is the surface of the meniscus, that is,

$$S_{l,v} = 2\pi R[R - (R^2-r^2)^{\frac{1}{2}}] = \frac{2\pi r^2}{\sin^2\beta}(1 - \cos\beta) \qquad \text{(Eq. 5)}$$

and,

$$dS_{l,v} = 4\pi r \frac{(1-\cos\beta)}{\sin^2\beta} dr \qquad \text{(Eq. 6)}$$

The total volume of mercury intruded is the volume of frustum between FK and GH and the volume under the meniscus. Thus:

$$V = V(\text{frustum}) + V(\text{meniscus}) \qquad \text{(Eq. 7)}$$

where,

$$V(\text{frustum}) = \frac{\pi\overline{CE}}{3}(r_1^2+rr_1+r^2) + \frac{\pi\tan\alpha}{3}(r_1-r)(r_1^2+r_1r+r^2) \qquad \text{(Eq. 8)}$$

and,

$$V(\text{meniscus}) = \frac{\pi R}{6}(1-\cos\beta)[3r^2+R^2(1-\cos\beta)^2] \qquad \text{(Eq. 9)}$$

which simplifies to:

$$V(\text{meniscus}) = \frac{(1-\cos\beta)(2+\cos\beta)}{\sin\beta(1+\cos\beta)} \qquad \text{(Eq. 10)}$$

As mercury intrudes further, the change in the total volume can be obtained by substituting Equations 8 and 10 into Equation 7 and differentiating,

$$dV = \left[-\tan\alpha + \frac{(1-\cos\beta)(2+\cos\beta)}{\sin\beta(1+\cos\beta)}\right] \pi r^2 dr \qquad \text{(Eq. 11)}$$

Substitution of Equations 4, 6 and 11 into Equation 1 and cancellation of $\pi r dr$ gives:

$$\frac{P}{\gamma_{l,v}} r = \frac{\frac{4(1-\cos\beta)}{\sin^2\beta} + \frac{2\cos\theta}{\cos\alpha}}{\frac{(1-\cos\beta)(2+\cos\beta)}{\sin\beta(1+\cos\beta)} - \tan\alpha} \qquad \text{(Eq. 12)}$$

which simplifies to:

$$\frac{P}{\gamma_{l,v}} r = -2 \sin(\alpha+\theta) \qquad \text{(Eq. 13)}$$

Consequently, Equation 13 gives the relationship between the intrusion pressure and the radius of a cone in terms of the slope of the cone and the angle of contact. It may be noted that Equation 13 becomes equal to Washburn equation when α equals 90 degrees, i.e., the cone converts to a cylinder.

If the change in the surface area of the meniscus is neglected as suggested by DeWit and Scholten (10), Equation 12 would be:

$$\frac{P}{\gamma_{l,v}} r = \frac{\frac{2\cos\theta}{\cos\alpha}}{\frac{(1-\cos\beta)(2+\cos\beta)}{\sin\beta(1+\cos\beta)} - \tan\alpha}$$

which simplifies to:

$$\frac{P}{\gamma_{l,v}} r = \frac{2\cos\theta\sin\beta(1+\cos\beta)}{2\cos\alpha+\cos\theta(1+\cos\beta)} \qquad \text{(Eq. 14)}$$

A further simple equation could be derived by assuming the meniscus to be a flat surface and neglecting the change in its surface area. Then, $dS_{s,v}$ is expressed by Equation 4; $dS_{l,v}$ is zero; and,

$$dV = \frac{d}{dr}[V(\text{frustum})]dr = -\pi r^2 \tan\alpha \, dr$$

Substituting these into Equation 1, and simplifying, the following relationship is obtained:

$$\frac{P}{\gamma_{l,v}} r = -\frac{2\cos\theta}{\sin\alpha} \qquad \text{(Eq. 15)}$$

which converges to Washburn equation when α equals 90 degrees.

Obviously, for a porous material, unless there is a characteristic α angle which can be determined by electron microscopy or some other means, Equation 13 cannot be used, and it will be necessary, although inaccurate, to apply Washburn equation in converting the test data to a pore-size distribution curve. Table 1 shows the values of the dimensionless constant $Pr/\gamma_{l,v}$, corresponding to the solutions of Equations 13, 14, 15 and Washburn equation for various θ and α angles. The percentages of error made by using the latter three equations are also tabulated.

Table 1 shows that, when the approximate equations are used, the error increases as α decreases from 90 degrees, i.e., errors are larger for less steep sided cones. The error also increases with decreasing contact angle. The value of the dimensionless constant is overestimated by the approximate equations in all cases. This will result in the overestimation of the pore size since $\gamma_{l,v}$, θ and α are constant for a given material and the intrusion pressure is an experimentally controlled

Table 1. Comparison of Equations 13, 14, 15 and Washburn equation

θ	α	Values of $Pr/\gamma_{l,v}$ and percent error (in parentheses)			
		Equation 13	Equation 14	Equation 15	Washburn Eq.
140°	89°	1.50942	1.55212 (2.83%)	1.53232 (1.52%)	1.53209 (1.50%)
140°	75°	1.14715	1.82509 (59.10%)	1.58614 (38.27%)	1.53209 (33.56%)
130°	89°	1.25864	1.29831 (3.15%)	1.28577 (2.16%)	1.28558 (2.14%)
130°	75°	0.84524	1.46346 (73.14%)	1.33093 (57.46%)	1.28558 (52.10%)
120°	89°	0.96962	1.00712 (3.87%)	1.00015 (3.15%)	1.00000 (3.13%)
120°	75°	0.51764	1.09347 (111.24%)	1.03528 (100.00%)	1.00000 (93.19%)

variable. Therefore, the error is reflected in pore size which is calculated from the values given in Table 1 and measured pressures.

It is seen in Table 1 that the greatest error is made when the assumption suggested by DeWit and Scholten (10) is adopted. This shows that the change in the area of the liquid-vapor interface cannot be neglected when pores with tapering cross-sections are being intruded by nonwetting fluids.

Table 1 also shows that the smallest error is made by using Washburn equation as compared to the other two approximate equations. When Washburn equation is employed to approximate a conical pore system, each section of the cone will be calculated as a cylinder of a greater radius; hence the pore-size distribution curve will be shifted to larger sizes.

The amount of shifting depends on the contact angle and the steepness of the cone; the smaller the contact angle and the less steep the cone, the greater the shift. Obviously, between two cones of equal base radii and different height or steepness, the less steep cone has a smaller volume, therefore its contribution to cumulative pore volume will be smaller, thereby making the net effect of the error smaller.

The values of $Pr/\gamma_{l,v}$ calculated by Equation 13 decrease as the sum of θ plus α decreases, as seen in Table 1. When θ plus α equals 180 degrees the dimensionless constant will be zero and with further decrease will have negative values. Since $\gamma_{l,v}$ and r cannot be negative, pressure must be negative for θ plus α smaller than 180 degrees. In other words, the pressure required for intrusion under such conditions is smaller than zero absolute, or is a tension. Consequently, during a porosimeter test, when mercury encounters the base of a cone of slope α smaller than $180 - \theta$, regardless of its size, the cone will be instantaneously and completely intruded without requiring the application of any positive pressure on mercury. This phenomenon cannot be observed in a large cone in the laboratory because of the effect of gravity on mercury; however, the effect of gravity on very small volumes of mercury intruding the pores of sizes encountered in mercury intrusion porosimetry measurements is negligible. The effect of this phenomenon on the pore-size distribution curve will be a shift to larger sizes than actual pores, since these cones may be intruded at much lower pressures than the intrusion pressures of the cylinders of corresponding sizes.

A spherical pore must have an open end in order to be available for the intrusion of mercury; therefore, spherical segments must be considered in this discussion. As shown in Figure 2, a segment can be visualized to be formed by many frustums of slope α changing with the curvature of the sphere. The bases of the frustums are parallel to the entrance of the segment and they have an infinitesimally small height Δh. The radius of the sphere is R, the radius of the entrance of the segment is r, and the slope of the frustum representing the entrance is α, as shown in Figure 2. The intrusion of the entrance is governed by Equation 13, which can be expressed as:

$$P = - \frac{2\gamma_{l,v}\sin(\theta+\alpha)}{R\sin\alpha} \qquad \text{(Eq. 16)}$$

where the entrance radius, r, is replaced by $R\sin\alpha$.

After the intrusion of the entrance frustum or slice, the second slice will spontaneously be intruded, because the pressure required for its intrusion is smaller than the pressure applied to intrude the entrance. This can be shown by expressing the variable term in Equation 16 as:

$$\frac{\sin(\theta+\alpha)}{\sin\alpha} = \cos\theta - \frac{\sin\theta}{\tan\alpha}$$

which has a decreasing value as α decreases from 180 to zero degrees. Since every following slice has a smaller α than the preceding one, a spherical pore will be instantaneously and completely intruded upon intrusion of the entrance according to Equation 16. The total volume of the pore will be expressed as a uniform pore of a size equivalent to the

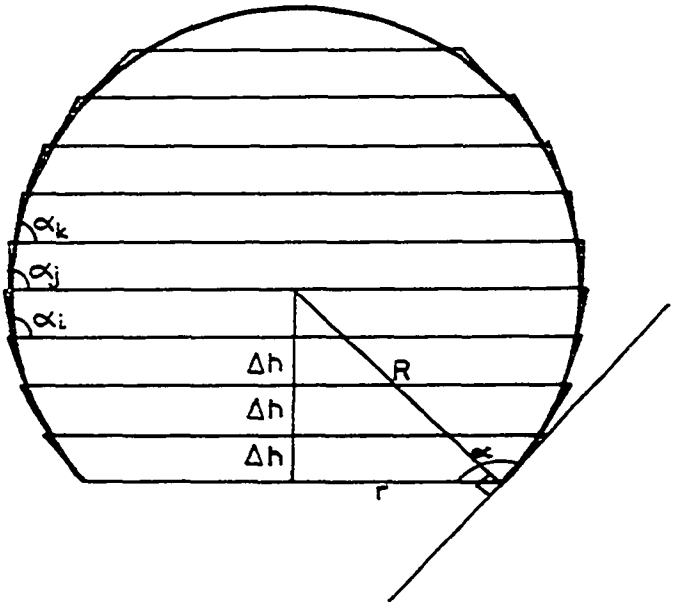

Figure 2. Representation of a spherical segment by frustums

entrance radius. Hence, the shift of the pore size distribution curve depends on the radii of the entrance and the sphere.

The Capillarity Approach

As an alternative method to balancing the surface free energies involved, the pressure drop across the liquid-vapor interface may be solved to analyze the intrusion of nonwetting fluids into pores of various shapes. This latter approach helps to better visualize the effect of contact angle and the slope of tapering pores.

The equation of Young and LaPlace states that:

$$\Delta P = \gamma_{l,v} \left(\frac{1}{R_1} + \frac{1}{R_2}\right) \qquad \text{(Eq. 17)}$$

where ΔP is the pressure drop across a curved surface defined by the two radii of curvature R_1 and R_2 on any two orthogonal planes. In case of spherical segments $R_1 = R_2 = R$, and Equation 17 becomes:

$$\Delta P = \frac{2\gamma_{l,v}}{R} \qquad \text{(Eq. 18)}$$

Equation 18 can be solved for the capillary depression in a cylinder. As shown in Figure 3, the radius of the cylinder, r, is related to the radius of curvature of the meniscus, R, by:

$$r = R\cos(180 - \theta) = -R\cos\theta \qquad \text{(Eq. 19)}$$

Substitution of the above into Equation 18 gives:

$$\Delta P = -\frac{2\gamma_{l,v}\cos\theta}{r} \qquad \text{(Eq. 20)}$$

which is the same relationship as Washburn equation. However, it should be realized that during the course of porosimeter tests, equilibrium is

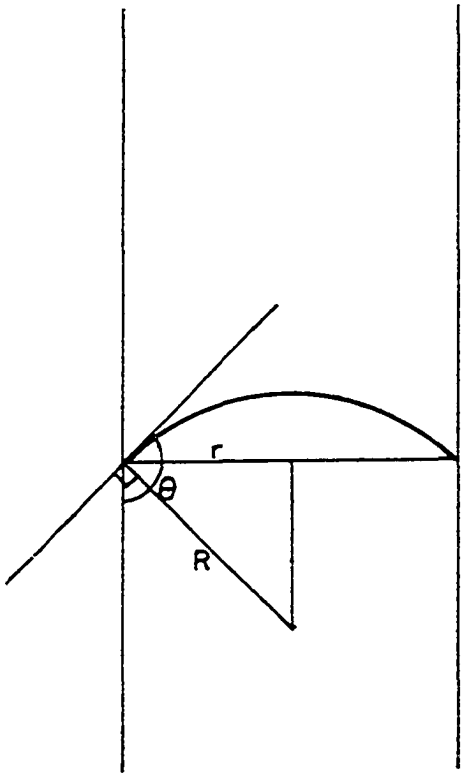

Figure 3. Intrusion of a cylindrical pore

reached instantaneously (14) upon intrusion of the evacuated cylindrical pore so that the pore is completely filled with mercury. Equation 20 holds only during the advance of the meniscus in the cylinder; and upon completion of the intrusion the meniscus disappears and Equation 20 does not apply.

The relationship between the radius of curvature of the meniscus, R, accommodated in a cone, at a cross-section of radius, r, as shown in Figure 1 is:

$$r = R\sin(\theta + \alpha) \qquad \text{(Eq. 21)}$$

and substituting into Equation 18 gives Equation 13 for the intrusion of a cone. Hence, surface energy and capillarity approaches result in the same relationship and the approximate equations derived in the preceding section are not justified.

During the intrusion of a conical pore, the mercury meniscus must contact the sides always at θ. If the summation of θ and α is smaller than 180 degrees, by simple geometry, the meniscus must be such that the vapor and liquid phases must be on the concave and convex sides, respectively; and, according to Young and LaPlace equation, the pressure must be higher on the vapor side. However, at room temperature, the pressure of the vapor phase is the vapor pressure of mercury which is about 1.6×10^{-3} N/m^2 (1.2 μm Hg), whereas the pressure on the liquid side is at least equal to the height of the mercury column on the sample placed in the porosimeter sample cell. Hence, the mercury meniscus described above can not be stable and such a cone will be instantaneously and completely intruded and the meniscus will disappear. When θ plus α equals 180 degrees,

the meniscus must be a plane surface, across which a pressure difference cannot exist, thus complete intrusion will take place. It should be realized that when α is slightly greater than 180 - θ, a major part of the cone will be intruded at a very small pressure; but, complete intrusion cannot be achieved regardless of how high a pressure is applied, because the tip of the cone can accommodate a meniscus with a very small radius of curvature.

The radius of curvature of a meniscus making a contact angle, θ, with a spherical segment has the minimum value at the entrance of the segment. Therefore, the segment will be instantaneously and completely intruded upon intrusion of the entrance, because less and less pressure is needed to intrude the following sections. It should be noted that, if the entrance of the segment is such that α is equal to or smaller than 180 - θ, the segment will be intruded without applying any pressure on mercury. If the entrance of the segment is such that α is slightly greater than 180 - θ, the segment will be intruded at a very low pressure. However, contrary to a cone of equal θ and α, the segment will be completely intruded and the meniscus will disappear. This is due to the continuously decreasing value of α which will eventually be smaller than 180 - θ in the sphere.

It is seen that surface energy and capillarity approaches result in the same conclusions governing the intrusion of cylindrical, conical and spherical pores. The intrusion of rectangular or slit like pores is essentially similar to a cylinder, if it is realized that the controlling radius of curvature is on the plane of the smaller width. It can be shown

by surface energy or capillarity approach that the pressure required to intrude a rectangular pore of entrance width, b, and depth, d, (b greater than d) is given by:

$$P = - \frac{2\gamma_{l,v}(b+d)\cos\theta}{bd} \qquad \text{(Eq. 22)}$$

which simplifies to:

$$P = - \frac{2\gamma_{l,v}\cos\theta}{d} \qquad \text{(Eq. 23)}$$

for slit-like pores where the width is much greater than the depth.

The pore shapes considered above can provide a satisfactory model to approximate the pore structure of porous materials. Assumptions of other pore shapes is not warranted because of innumerable possibilities and lengthy and complicated computations required for the solutions of Equations 1 or 17. It may be realized that the geometric definition of the mercury meniscus in tapering pores is required since it was shown that the change in the liquid-vapor interfacial area cannot be neglected.

Analysis of Hysteresis

As mentioned earlier, mercury intrusion porosimeter tests result in pressurization and de-pressurization curves which do not coincide in shape nor in total amount of mercury intruded and withdrawn. Ritter and Drake (24) reasoned that, if the pores of the specimens were either uniform in diameter or V-shaped, mercury would be expected to flow out when the applied pressure was released. However, the ink-bottle pores would not empty upon releasing the pressure, because mercury at the entrance would be ejected at a higher pressure than that corresponding to the ejection of

mercury in the wider portion. This results in breaking the contact of mercury in the main portion of the pore with the mercury in the chamber; consequently, mercury will be retained in the ink-bottle pore even when the pressure is released completely.

Although Frevel and Kressley (14), and DeWit and Scholten (10) adopted the above explanation, Quynn (23) proposed a quantitative explanation by stating that, "Any pore volume element of mean diameter larger than the diameter of the single channel by which it communicates to the outside surface will not empty on de-pressurization." And considering some idealized models, he predicted that, "The de-pressurization curve should have roughly the same shape as pressurization curve, i,e., the inflections should occur at the same pressure in both curves." Quynn's conclusions are incorrect as will be explained later.

Kruyer observed hysteresis in his experiments on samples of packed spheres (16). Caro and Freeman (8) considered hysteresis to be the combined effect of the difference between advancing and receding contact angles and irreversible chemisorption of mercury on the pore walls. Mayer and Stowe (20) applied the above explanations to the model of packed spheres, but concluded that, "The basis for judging the validity of these various speculations is not evident, and it appears that withdrawal and hysteresis are neither simple nor completely understood."

Watson et al. (31) proposed that, if the mercury meniscus in a uniform pore disappears due to complete intrusion of a closed ended pore or the coalescence of the two advancing menisci in an open ended pore, the force that causes the ejection of mercury from such pores would be

removed. Hence, mercury could be retained in a uniform radius pore as well as in an ink-bottle pore. This reasoning considers the pressure drop across meniscus as the only factor governing the withdrawal of mercury from the pores and fails to realize the effect of surface free energies involved.

Hill (15) proposed that adhesion tension between the surfaces of mercury and pore walls acts against the applied pressure and will cause the ejection of mercury from a completely filled pore. He postulated that at a critical pressure, P_e, mercury column severs itself from the wall of the pore by radially moving an infinitesimal distance dr. Hill called this phenomenon "collapse" and established the following relationship:

$$P_e dV - \gamma_{l,v} \cos\theta dS = 0 \qquad \text{(Eq. 24)}$$

where dV and dS are the changes in the volume and surface area of the mercury column, respectively, due to radial motion. The first term in Equation 24 is the work done against the external pressure and the second term is adhesion tension (l) which represents the change in surface free energy. For a cylindrical column of radius, r, and length, h, dV and dS can be expressed as:

$$dV = \frac{d}{dr}(\pi r^2 h)dr = 2\pi rh\ dr \qquad \text{(Eq. 25)}$$

$$dS = \frac{d}{dr}(2\pi rh)dr = 2\pi h\ dr \qquad \text{(Eq. 26)}$$

Substituting Equations 25 and 26 into Equation 24, Hill obtained the following relationship for the ejection pressure of mercury from a cylinder of radius r:

$$P_e = \frac{\gamma_{l,v}\cos\theta}{r}$$

with the sign convention of the author of this study, the above equation is:

$$P_e = -\frac{\gamma_{l,v}\cos\theta}{r} \qquad \text{(Eq. 27)}$$

It should be emphasized that Equations 25, 26 and 27 are valid only during the collapse and do not govern an equilibrium withdrawal of mercury from the pore after collapse takes place.

Hill (15) supports the validity of Equation 27 with experimental evidence obtained by intruding mercury into artificial pores of known diameter. A qualitative experiment performed by the author of this study also demonstrated the ejection of mercury from a completely filled capillary. A thick-wall glass capillary tube was filled with mercury and placed in a mercury container. The capillary was immersed horizontally in mercury only 10^{-3} - 2 x 10^{-3} m deep so that the mercury column in the tube could be observed from the top. The mercury container was placed in a vacuum desiccator and evacuation was started to eliminate the atmospheric pressure. When vacuum in the desiccator improved within a few minutes of evacuation, the mercury column in the capillary tube was ejected, indicating that the ejection pressure was equal to the height of mercury column on the capillary tube.

Comparison of Equation 27 with Washburn equation shows that mercury will be ejected from a completely filled cylindrical pore when the ejection pressure is half the pressure applied to intrude the same pore. Hence, the pressurization and de-pressurization curves cannot coincide

even if the sample contains no ink-bottle pores, but has some uniform pores that are completely intruded. In that case the total amount of mercury intruded and withdrawn must be equal if chemisorption is negligible.

When collapse of the mercury commences at the narrowest cross-section of a nonuniform pore, the mercury column along the length of the pore having a diameter equal to or less than twice the diameter of the narrowest section will be ejected, because the outside pressure is already reduced to the level which will permit its ejection. Consequently, a "uniform cylindrical pore" is defined as a pore having a cross-section with a diameter range equal to or less than twice the diameter of its narrowest cross-section, i.e., $r_{min} < r < 2r_{min}$, where r_{min} is the radius of the narrowest neck calculable using Equation 27, and r represents the radius range of a pore which is indistinguishable from a uniform pore with a constant radius r_{min}.

Using a theoretical derivation similar to that used for cylindrical pores, Hill (15) calculated the ejection pressure for rectangular pores. For a rectangular pore of width b and depth d, the ratio of penetration pressure to ejection pressure is 1 + d/b. For slit-like pores where b is very much greater than d, the ratio of penetration to ejection pressure should approach unity.

It is very likely that the closed end of cylindrical pores may not be a plane circle as the base of a cylinder, but be approximated by a cone or a segment of a sphere. The conditions for complete or incomplete intrusion of pores was discussed earlier. If α is greater than 180 - θ, so

that the tip of the cone cannot be intruded even at the highest pressures applied, withdrawal of mercury from the pore will follow Equation 13. Hence, mercury column in a cylinder extending from the base of such a cone will be withdrawn at the intrusion pressure due to the presence of a meniscus in the cylinder. However, if α is equal to or smaller than $180 - \theta$, it was shown that the cone will be completely intruded at zero or negative pressures, and the meniscus will disappear. Hence, a "collapse" as proposed by Hill for cylinders or rectangles cannot take place in a cone unless a suction is applied. Consequently, mercury in a completely intruded cone will be trapped at the end of de-pressurization. It should be realized that formation of a meniscus concave toward the cone is thermodynamically stable according to Young and LaPlace equation when α is smaller than $180 - \theta$. Similarly, collapse cannot take place in a spherical pore since α is always smaller than $180 - \theta$ at some portion of the surface which will not release mercury unless a suction is applied. Hence, all spherical pores will retain mercury at the end of de-pressurization. This conclusion is supported by experimental evidence which will be presented in the following sections.

Table 2 summarizes the results of the above analyses showing various pore shapes, intrusion and withdrawal expressions. The influence of the physicochemical factors mentioned in the literature and the derivations of the intrusion and withdrawal pressures for various pore shapes illustrate the complexity of interpreting the intrusion curves as well as the hysteresis from mercury intrusion porosimetry. Washburn equation is the best approximation, from a practical point of view, in converting the test

Table 2. The relationships for the intrusion and withdrawal of mercury from various pore shapes

Pore shape	Expression relating intrusion pressure to pore size	Upon approximation by Washburn eq. the pore-size distr. curve shifts to	Description of withdrawal or retention
Cylinder	$P = -\frac{2\gamma\cos\theta}{r}$	-	Same as intrusion if meniscus exists. Otherwise: $P_e = -\gamma\cos\theta/r$
Regular prism	$P = -\frac{2\gamma(b+d)\cos\theta}{bd}$	-	Same as intrusion if meniscus exists. Otherwise: $P_e = -2\gamma\cos\theta/d$
Slit-like (b>>d)	$P = -\frac{2\gamma\cos\theta}{d}$	-	Same as intrusion.
Ink-bottle	$P = -\frac{2\gamma\cos\theta}{r(\text{entrance})}$	Smaller pore sizes	Entrance ejects at $P_e = -\gamma\cos\theta/r$ The main portion retains mercury.
Cone	$P = -\frac{2\gamma\sin(\theta+\alpha)}{r}$	Larger pore sizes	Same as intrusion if $\theta + \alpha > 180°$ Mercury retained if $\theta + \alpha \leq 180°$
Spherical segment	$P = -\frac{2\gamma\sin(\theta+\alpha)}{r(\text{entrance})}$	Larger or smaller pore sizes depending on α	Mercury retained

data to a pore-size distribution curve. However, many samples will contain the various pore shapes, shown in Table 2 with their effect on pore size distribution curves; therefore, the results obtained by Washburn equation must be evaluated accordingly. As a simple example, consider a conical pore system of α equal to 75 degrees and a contact angle, θ, of 130 degrees. When the test data obtained on such a sample are converted to a pore-size distribution curve using Washburn equation, the curve will indicate the pore sizes as 52.10 percent greater than the actual value as shown in Table 1, last column. In other words, the cumulative intrusion at a radius of x m will be shown at 2x m. It should also be mentioned that the meaning of the de-pressurization curve is limited to estimating the total volume of ink-bottle pores in the sample.

The Second Intrusion Method

Another approach to the problem of refining the interpretations of the pore-size distribution curves drawn by treating the test data with Washburn equation is to intrude the specimen a second time to determine the distribution of uniform pores. Hill (15) and Caro and Freeman (8) reported second intrusion curves. Hill used the data to calculate the specific surfaces of fired clays and compared the results with nitrogen adsorption data. Caro and Freeman made no use of their curves.

Mercury contaminating the pore walls of the specimen during the first intrusion may change the contact angle and lead to errors in computations of pore size. Similarly, chemisorption might be misinterpreted as mercury

retained in ink-bottle pores. These factors can be neglected because the second intrusion method cannot detect small variations in pore sizes.

The second intrusion can improve the interpretation of the pore geometry of materials. This will be shown in this study by illustrating the intrusion, de-pressurization, and re-intrusion of two hypothetical samples. Two hypothetical samples designated s-1 and s-2 are shown in Figure 4a. The two specimens have equal porosities and equal entrance diameters to all pores, however, the shapes of two of the pores are different. For the purposes of discussion all the pores are numbered, and in the text, individual pores will be referred to as p-1, p-2, p-3, etc. Thus, in Figure 4a, pores p-4 and p-5 are of different shapes in the two specimens. To avoid complications, all pores are assumed to have circular cross-sections, so that any vertical section through the specimen would result in the cross-sections shown in Figures 4-6. The tapered sections should not be visualized as cones, but as cylinders of increasing or decreasing radii with very small heights. Again for simplicity, the cross-sectional pore area rather than pore volume will be discussed. It is assumed the pore distribution of these two specimens is measured with a porosimeter which has maximum pressure capacity for intruding pores down to a diameter of just larger than one unit. The mercury intrusion pore-size distribution curves of the two specimens will be identical; whereas, the true pore-size distributions of the two specimens are in fact different.

Figure 4a shows the specimens surrounded by mercury in the sample cell. The specimens do not contain any large pores that would be intruded before the application of the first pressure increment. For

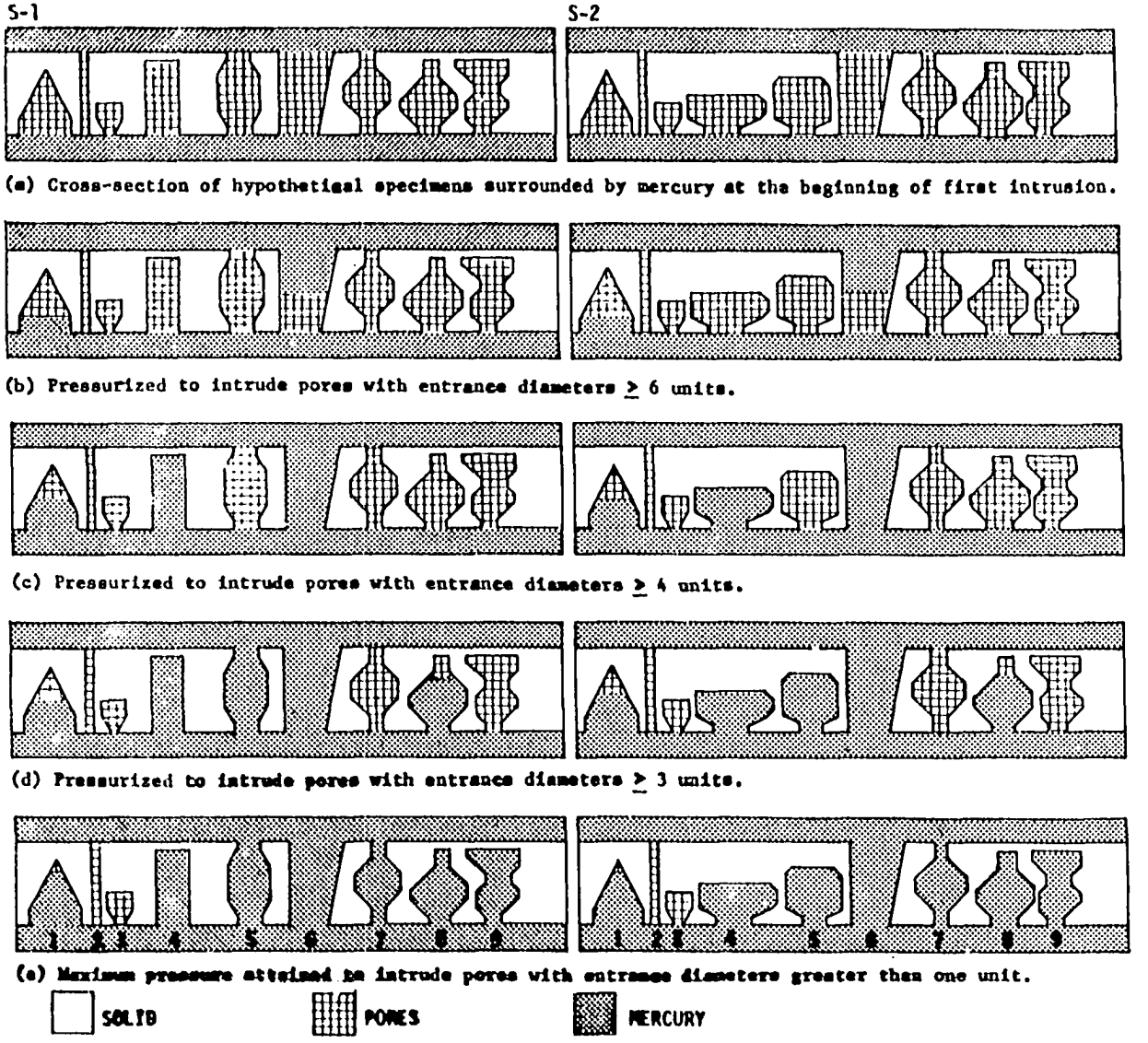

Figure 4. Schematic diagram of the first intrusion

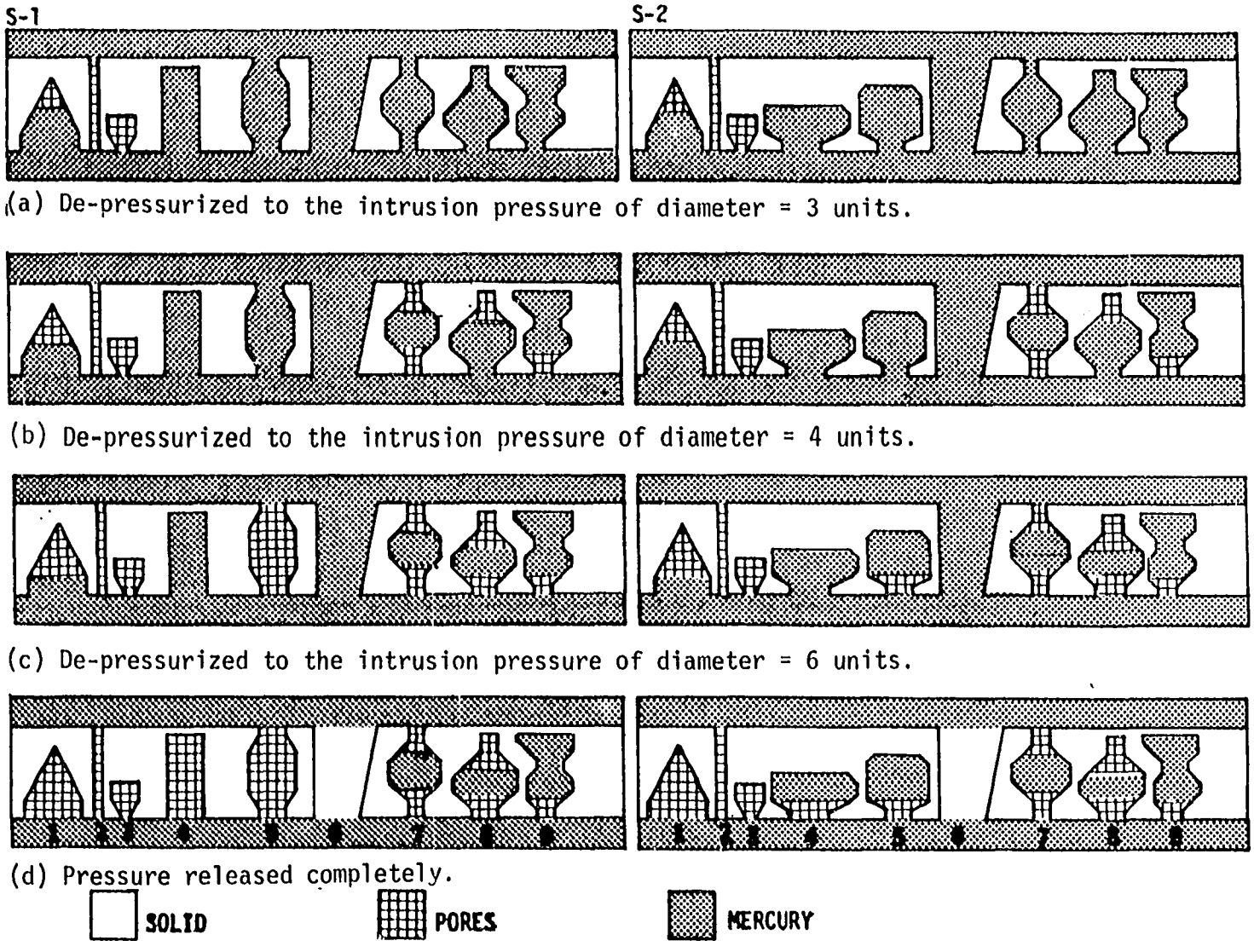

Figure 5. Schematic diagram of de-pressurization

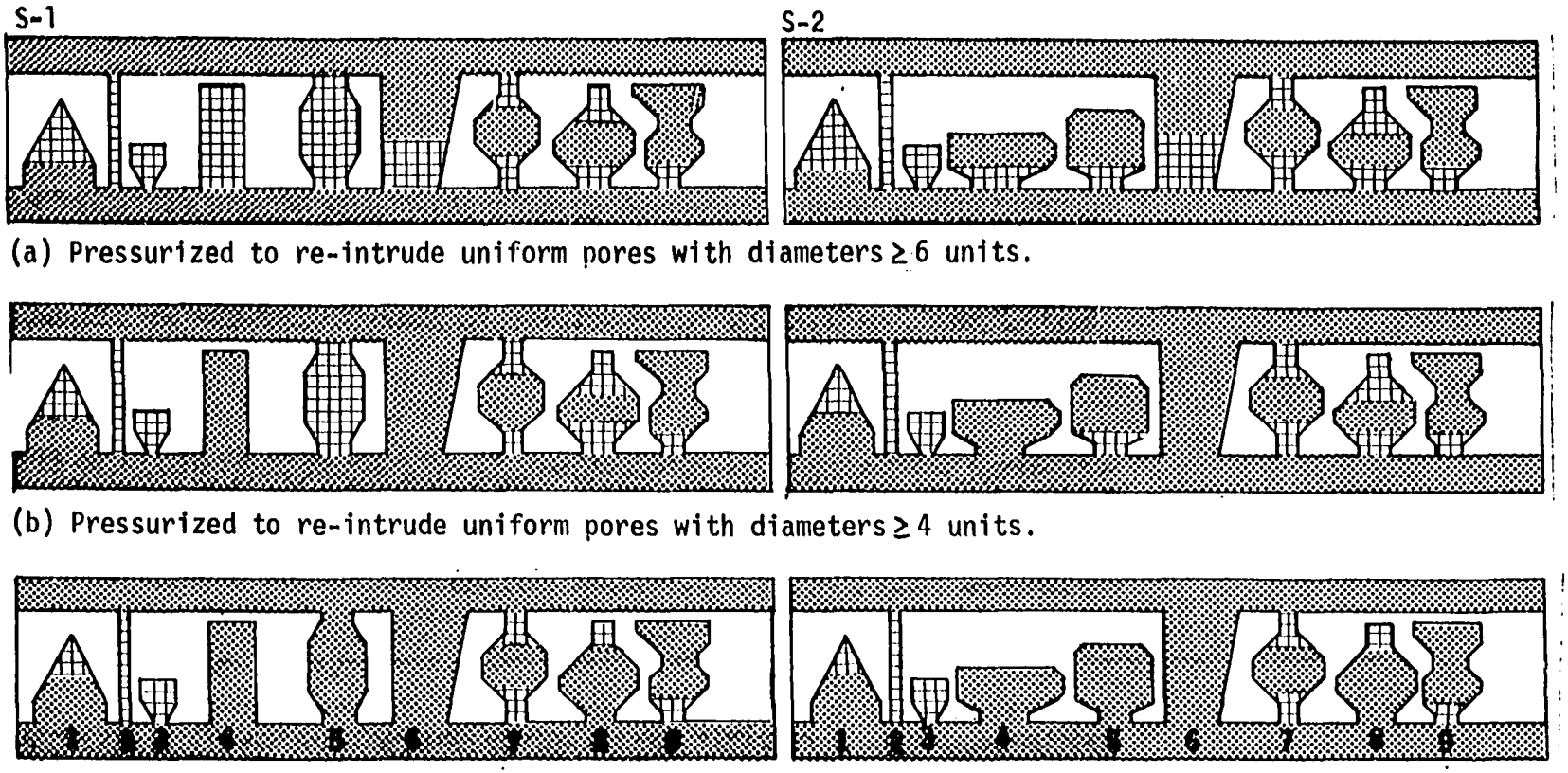

Figure 6. Schematic diagram of the second intrusion

convenience, mercury menisci are shown as straight lines rather than arcs in all subsequent drawings. Fractions of p-1 and p-6 are filled when the pressure is increased to intrude pores of diameter equal to or greater than 6 units as shown in Figure 4b. Note that p-8 and p-9 in s-1 and p-4, p-5, p-8 and p-9 in s-2 have some portions with diameters equal to or greater than 6 units, but they are not intruded at the corresponding pressures due to the narrower entrances into those sections. Figure 4c shows that p-4 is completely filled when the pressure is high enough and a total area of 36 units is recorded tc be in pores of diameter equal to 4 units. This is actually the case in s-1, whereas in s-2, the ink-bottle pore p-4, with a main portion of maximum diameter 9 units, is recorded as a uniform pore with a diameter of 4 units. Similar errors will occur as p-5, p-7, p-8 and p-9 are intruded as seen in Figure 4d and e. Parts of pointed tips of pores less than 1 unit in diameter as in p-1, small uniform pores as p-2, and larger ink-bottle pores with small necks like p-3 remain unintruded at the end of pressurization. Note that the cumulative first intrusion curves for both specimens will be the same although the true pore-size distributions are different. The pore-size distribution curves are shown in Figures 7 and 8.

Figure 5a shows the early stages of de-pressurization. The pressure on mercury is released to the intrusion pressure of diameter equal to 3 units and only the mercury surface in p-1 is retracted to the level where the diameter is 3 units. There is no change in other pores. In Figure 5b the pressure is further released to the intrusion pressure of diameter equal to 4 units and exactly at this point, mercury columns in the parts

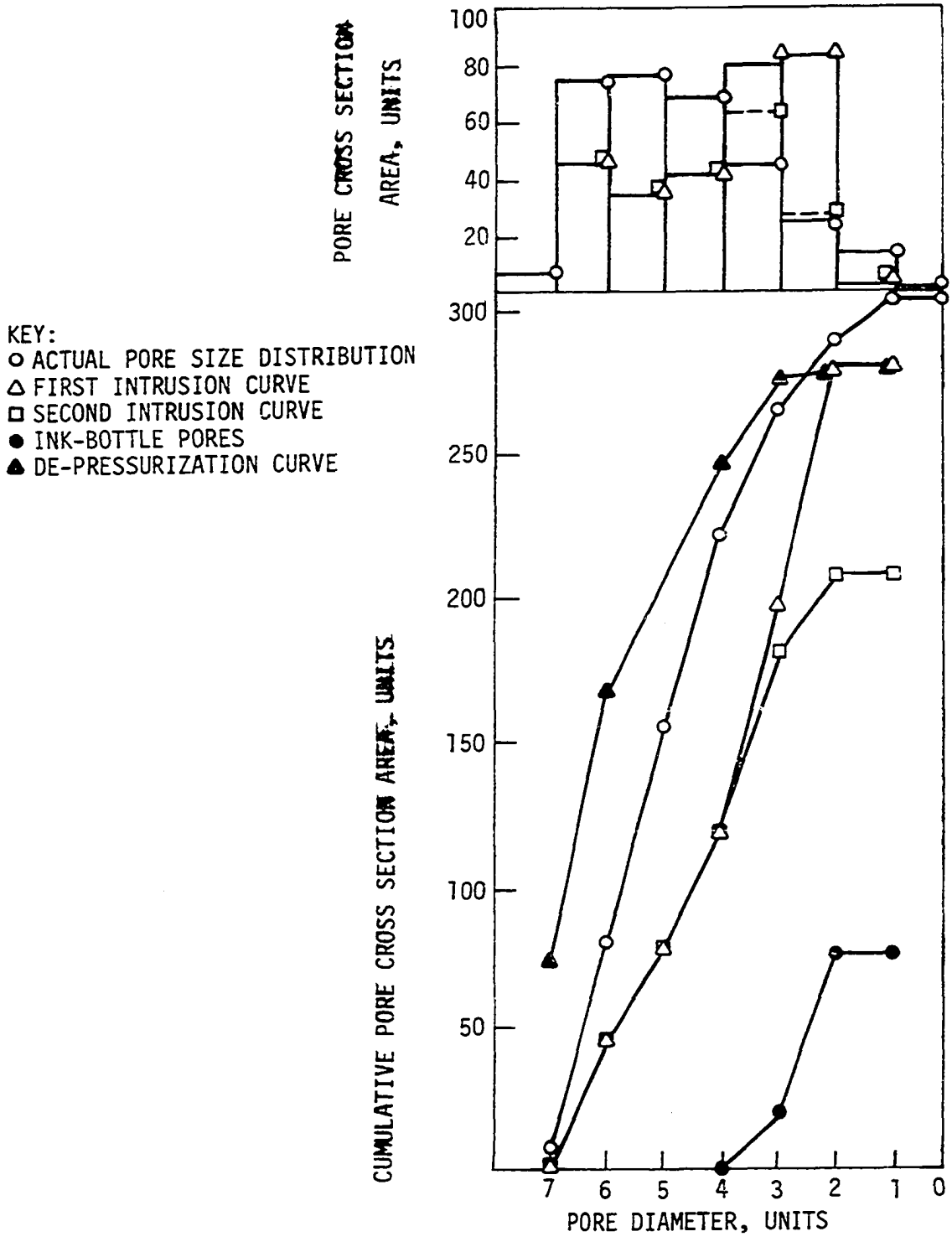

Figure 7. Pore-size distribution of hypothetical specimen S-1

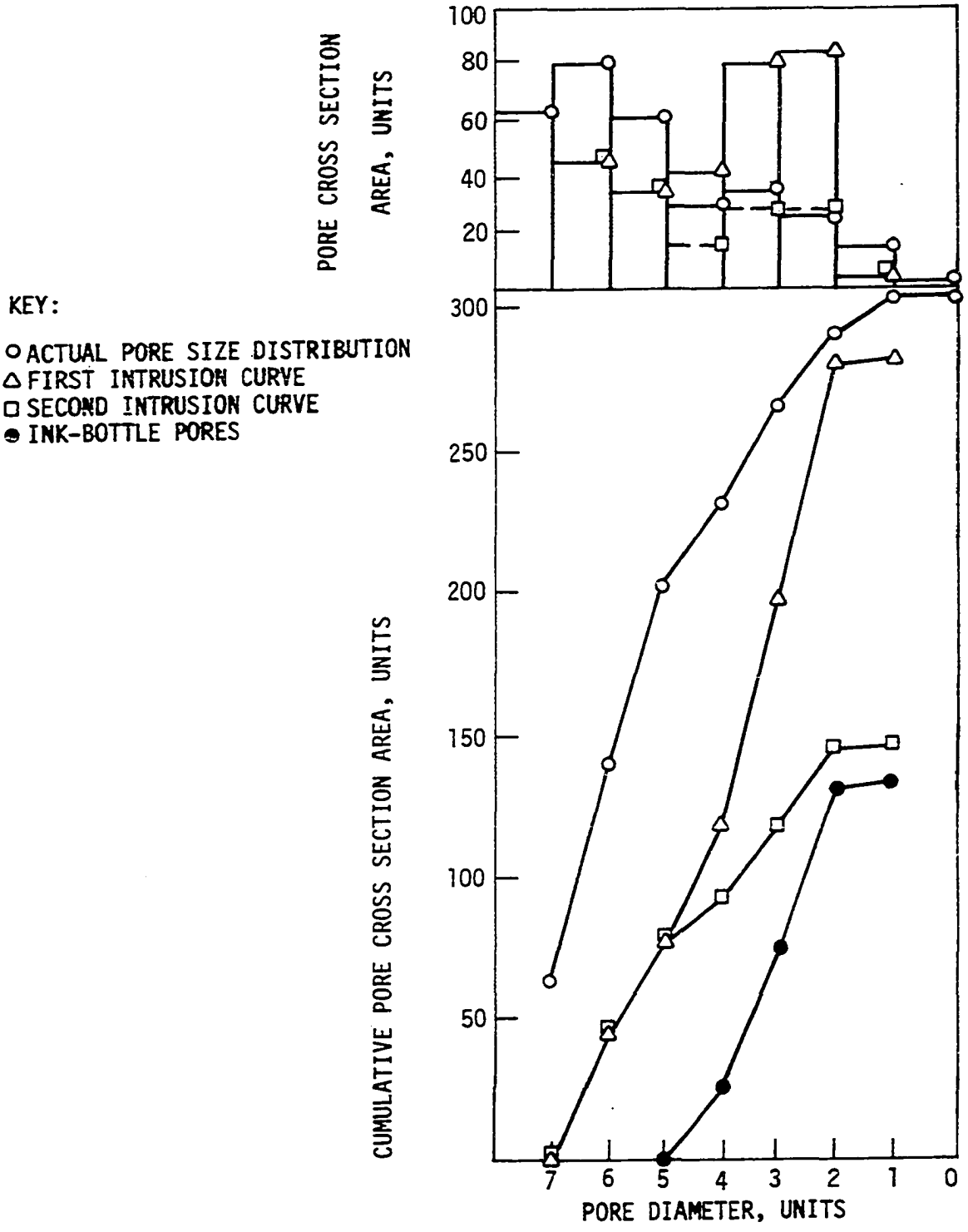

Figure 8. Pore-size distribution of hypothetical specimen S-2

of p-7, p-8 and p-9, where the diameter is equal to 2 units, collapse and the mercury is ejected from portions of these pores having diameters equal to or smaller than 4 units at retreating menisci. From this point on mercury in the main portions of p-7 and p-9 has lost contact with the outside and thus will not respond to further decreases in the outside pressure. Figure 5c shows that at a pressure equivalent to an intrusion diameter of 6 units, in s-1, mercury from the main portion of p-5, where the diameter is equal to 5 units, is ejected along with the entrance, where the diameter is equal to 3 units, because the variation in diameter is smaller than twofold. At this point, mercury at the entrances of p-8 of both specimens and p-5 of s-2 will collapse; thus the mercury in those pores loses contact with the outside and will not be ejected even though the pressure will be further reduced. As de-pressurization continues, mercury in p-4 and p-6 will be ejected at the intrusion pressures of diameters equal to 8 units and 10 units, respectively, but mercury will be retained at the portions of p-4 of s-2 where the diameter is greater than 8 units. Figure 5d shows the end of the de-pressurization cycle. Mercury retained in s-1 is 23.39% and in s-2 43.76% of the true total pore cross-sectional areas. However, from porosimetry measurements, it will be observed as 25.36% and 47.45% due to the unintruded pores, p-2 and p-3.

Figure 6 shows the second intrusion cycle where uniform pores and necks of ink-bottle pores are re-intruded; the total intrusion is less than the first intrusion by the amount of mercury retained in the sample at the end of the de-pressurization. The final step of second intrusion would be the same as Figure 4e. The steps shown in Figures 4e, 5 and 6

would be followed each time, if pressurization and de-pressurization are repeated.

Pore-size distributions of the hypothetical specimens are presented in Figures 7 and 8. Chemisorption is neglected and no alterations in the structure of the specimens are assumed. Contact angle of mercury and the specimen are assumed to be equal in the first and second intrusions. Obviously, the actual pore-size distributions cannot be determined by mercury intrusion porosimetry, although they are plotted in Figures 7 and 8 to show how close the first and second intrusion curves are approaching reality. The first intrusion curve is the same for s-1 and s-2, but by plotting the second intrusion curve the difference between the pore structures of the two specimens can be detected. It can then be concluded that both specimens have a total porosity of 279 unit squares (actually 302.5), but s-1 has 16.75 and 54 unit squares of ink-bottle pores with neck diameters of 3 and 2 units, respectively, whereas s-2 has 26, 52.375 and 54 unit squares of ink-bottles with neck diameters of 4, 3 and 2 units, respectively. Distribution of volume in ink-bottle pores intruded at each neck diameter can be plotted from the difference between first and second intrusion curves.

The conventional de-pressurization curve is plotted for s-1 in Figure 7. Note that the total amount of mercury retained in ink-bottle pores is the difference between the final points (diameters greater than 1 unit) of the first and second intrusion curves, which is also represented by the final point (diameter equal to 7 units) of the de-pressurization curve. In Figure 7 the hysteresis between first intrusion and de-pressurization

curves is large reflecting the fact that the pores are not slit-like but have circular cross-sections and most are completely filled at the end of intrusion. If many pores had unfilled tips like p-1 or were composed of slit-like shapes, the hysteresis loop would be smaller, although the final point of de-pressurization would be the same.

METHODS OF INVESTIGATION

The importance of the pore structure of hardened cement paste as related to the properties and behavior of concrete was mentioned in the introduction. Winslow and Diamond (33) determined the pore-size distributions of cement pastes mixed in vacuum with 0.4 and 0.6 water-cement ratios and hydrated in a saturated calcium hydroxide solution for various periods. They concluded that, "The results confirm the general concept that as a paste hydrates the total pore volume decreases and a general reduction in pore size takes place" (33). The same trend was observed with decreasing water-cement ratio. The existence of a threshold diameter for mercury intrusion in paste, and its decrease with decreasing water-cement ratio and increasing age were observed (33). Winslow and Diamond concluded that, "The threshold diameter corresponds approximately to the minimum diameter of channels that are essentially continuous through the paste at a given age" (33). Therefore the pores greater than the threshold diameter are discontinuous. In most pastes, the threshold diameter was in the range of 10^{-6} - 10^{-7} m. Bager and Sellevold observed that, "The threshold diameter is extremely sensitive to the exact details of the specimen preparation" (3).

On a fracture surface through air-entrained hardened cement paste, mortar, or concrete, typical air voids can be observed with a naked eye. Figure 9 shows a magnified (3x) photograph of a fracture surface through an air-entrained cement paste hydrated for 60 days. The air voids are essentially spherical in shape with diameters in the range of 5×10^{-4} -

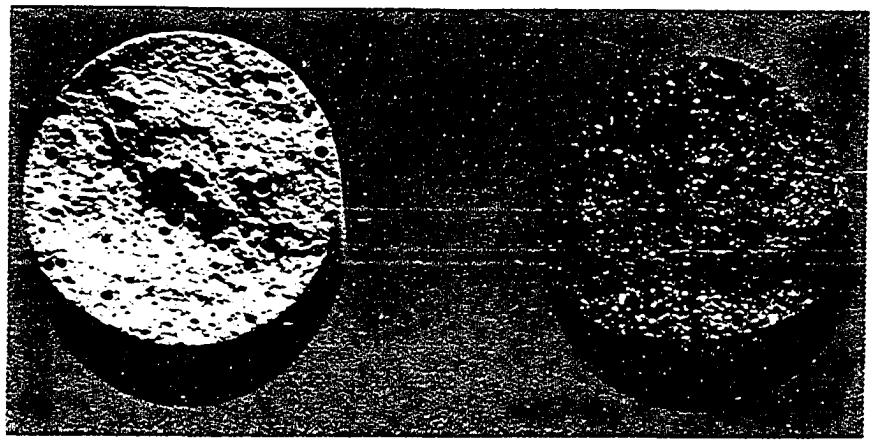

Figure 9. Fracture surfaces of air-entrained cement pastes of 60 days age, before porosimeter test (left), and after mercury intrusion (right).

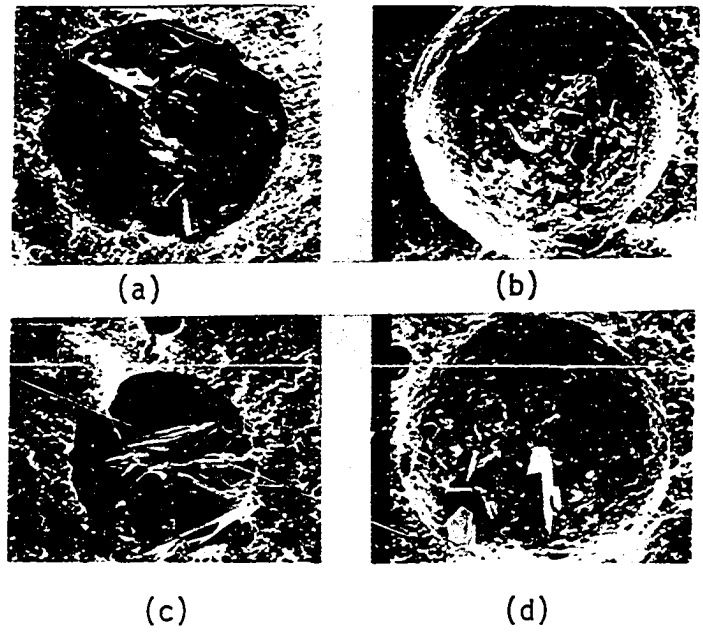

Figure 10. Calcium hydroxide crystals deposited in the air voids of air-entrained cement pastes:
(a) After 60 days of curing in saturated $Ca(OH)_2$ solution,
(b) After 60 days of curing in humidity room,
(c) After 130 days of curing in saturated $Ca(OH)_2$ solution,
(d) After 60 days of curing in water.

5×10^{-3} m. Figure 10 shows a close-up of the air voids taken by scanning electron microscope at 50x magnification. The formation of calcium hydroxide crystals will be discussed later.

The experiments in this study were designed to investigate the effect of air-entraining on the pore-size distribution of hardened cement paste by the second intrusion method. The main idea behind the approach was that the air voids will retain mercury at the end of first intrusion-depressurization cycle so that they will have no influence on the second intrusion curve. Hence, if air-entraining only introduces the air voids observed by a naked eye and has no other effect on the pore structure of hardened cement paste, the second intrusion curves of air-entrained pastes must be similar to the second intrusion curves of pastes containing no entrapped or entrained air, provided that the water-cement ratio and age of the two sets of pastes are equal. In order to test this hypothesis, a sample preparation procedure was established. Then, two sets of cement pastes were prepared; one set under evacuation and the other set using an air-entraining agent. The pore-size distributions were determined with the mercury intrusion porosimeter at various ages. Similarly, mortar samples were prepared and tested to compare the results with the pastes. The details of experimental procedures are presented in the following sections.

Materials Used

The cement used in this study was a commercial Type 1 Portland cement of specific gravity 3.17 and Blaine fineness 345 m^2/kg. The composition

was determined by the Bogue method as 59.58 percent C_3S, 15.45 percent C_2S, 8.98 percent C_3A, and 5.78 percent C_4AF.

Distilled water was used in preparing the samples and a commercial air-entraining agent, designated as Ad-Aire, was added to obtain air-entrained pastes and mortars. Standard Ottawa sand, as defined in ASTM C 109, was used in the preparation of mortar samples.

Preparation of Pastes

A clear definition of the sample preparation method is necessary, since the pore size distribution of hardened cement pastes is extremely sensitive to the details of mixing, molding and curing technique (3,26). In order to establish a sample preparation method that produces air-entrained and no-air pastes consistent among themselves and comparable with each other, four different batches of pastes were prepared in the first phase of the investigations. The water-cement ratio and age of these pastes were 0.6 and 3 days, respectively. The mixing, molding and curing procedures were as follows.

Air-entrained pastes were prepared by mixing 0.2 kg of cement with 1.20×10^{-4} m^3 of water containing the air-entraining agent. A kitchen mixer (Kitchen Aid Model K4-B) was used for mixing. All the mixing water was placed in the bowl, the cement was added and 30 seconds was allowed for the absorption of water. Then the batch was mixed at slow speed for one minute and allowed to stand for one and a half minutes. After standing, the mixing was completed by one minute mixing at medium speed.

The air content of the fresh paste was measured by a Chace Air Indicator as 6 percent. However, some air bubbles emerged to the surface while transferring the paste from the mixing bowl to the molds; therefore, the air content of individual samples varied. A portion of the fresh paste was poured into flat bottom glass test tubes of 0.015 m diameter and 0.050 m height. The other portion of the paste was placed in similar size vials with a spatula while agitating the vials by tapping the bottom on the bench. The caps were placed on full vials and the vials were turned upside down. Hence, two batches of air-entrained pastes, one unagitated and the other agitated, were obtained. The pastes were stored in a humidity room kept at 85±10 percent relative humidity and 28±2°C.

Samples containing no entrained or entrapped air were mixed in a vacuum desiccator modified for this purpose as shown in Figure 11. In addition to the outlet connected to a mechanical vacuum pump, two holes were bored on the lid. A Tiernan gauge was connected to the desiccator by a tube fixed to one hole and a mixing paddle was operated through an O-ring seal fixed into the second hole. For each sample, 0.005 kg cement and 3×10^{-6} m^3 of distilled water were placed in test tubes mentioned above. The tube was placed in a holder in the desiccator and the lid was closed, aligning the mixing paddle with the tube, so that the paste could be mixed by rotating the paddle in the tube. Then the vacuum pump was started and the air in the desiccator evacuated to an absolute pressure of 2.67×10^3 N/m^2 (20 mm of mercury). Naturally, water vapor was evacuated with the air; therefore, a petri dish of water was placed in the desiccator and the walls were kept wet to minimize loss of water from the paste

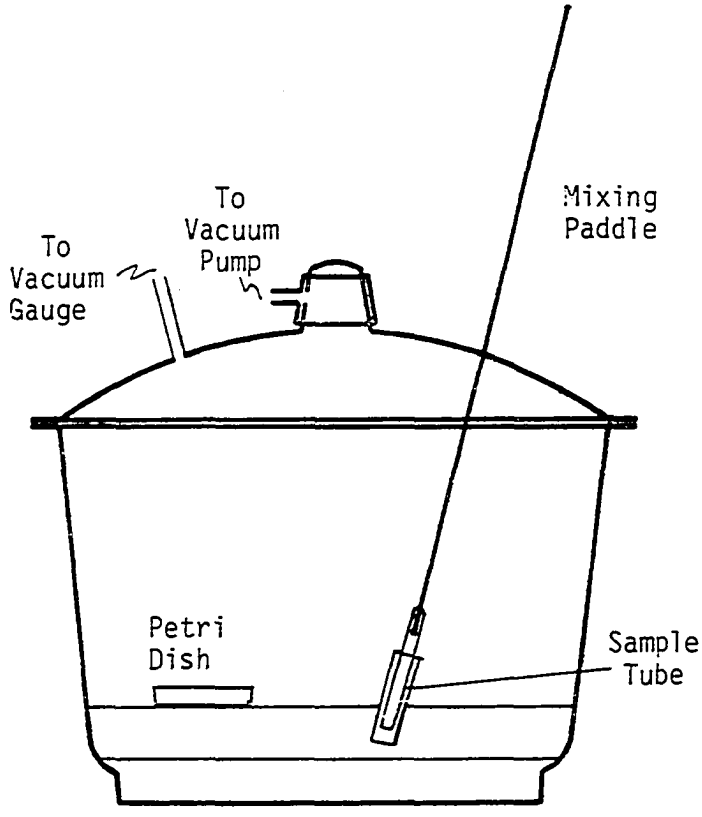

Figure 11. Diagram of modified vacuum desiccator used for mixing air-free cement pastes

so that the water-cement ratio was not reduced significantly. The pressure inside the desiccator was maintained below 2.67×10^3 N/m^2 throughout mixing. Upon completion of mixing, the vacuum was disconnected, the lid opened, and the tube containing the paste removed. Microscopic examination of the hardened paste indicated that this method produced a paste with no entrapped air. A portion of the pastes prepared as described above were allowed to harden in the tubes, and the remainder transferred into vials while agitating in a manner similar to the air-entrained pastes. The two batches of air free pastes, one unagitated and the other agitated, were also stored for three days in the humidity room.

The samples were removed from the humidity room at the end of the curing period, the tubes and vials were broken, and the hardened pastes dried at 105±5°C in an oven for at least 48 hours. Consequently four different pastes were obtained and are designated:

0.6/3d/A: This paste has a water-cement ratio of 0.6, an age of 3 days and is air-entrained.

0.6/3d/Ax: This paste is similar to the above, but it has undergone agitation during molding.

0.6/3d/AF: This paste also has a water-cement ratio of 0.6 and an age of 3 days, but was mixed under evacuation, therefore it is air-free.

0.6/3d/AFx: This paste is similar to the above, but it has undergone agitation during molding.

The pore-size distributions of the pastes were determined by the mercury intrusion porosimeter.

Mercury Intrusion Porosimetry

The instrument used in this study was Micromeritics Model 910 Mercury Penetration Porosimeter capable of exerting 3.45×10^8 N/m^2 (50,000 psi) pressure. The maximum pressures applied during this work were between 2.76×10^8 and 3.10×10^8 N/m^2 (40,000-45,000 psi). The compressibility of the system was corrected by using blank run results.

The samples tested were 1×10^{-3} - 3×10^{-3} kg pieces broken from the hardened pastes by discarding the top and bottom portions. The first intrusion and de-pressurization were performed during the day, and the samples were left in the porosimeter overnight to allow completion of the withdrawal of mercury from the pores. During pressurization, mercury meniscus at the precision bore tubing of the sample cell shown in Figure 12 retreats due to mercury intruding the pores. Hydraulic fluid follows the mercury surface, thereby contaminating the walls of the tubing. Upon de-pressurization the mercury meniscus advances due to withdrawal from uniform pores, however this takes place along the contaminated portion of the stem. Therefore, during second intrusion the mercury meniscus retreats along the contaminated tubing where the interface properties such as the contact angle may be different than the first intrusion. In order to eliminate this effect, the sample cell was removed from the pressure vessel and some mercury from the precision bore tubing withdrawn by a syringe, so that the meniscus was relocated at the uncontaminated section of the tubing. Then the sample cell was placed in the pressure vessel, hydraulic fluid refilled and the second intrusion test was performed.

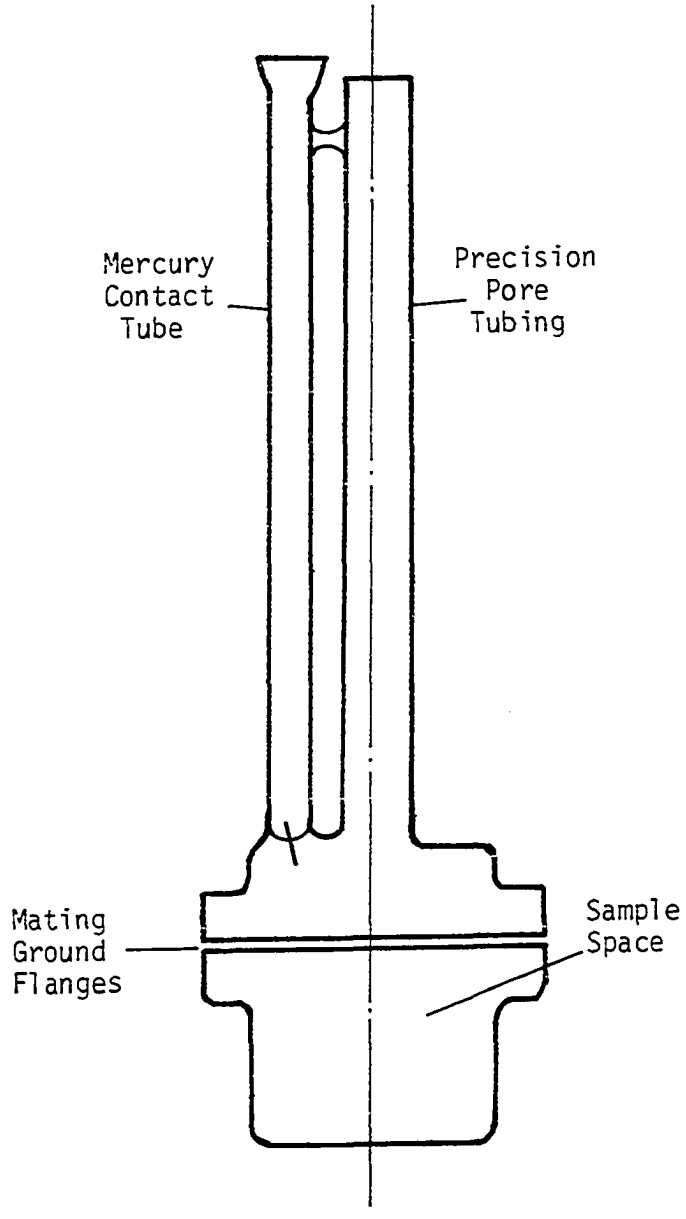

Figure 12. Porosimeter sample cell

Surface tension of mercury is taken as 48.4 N/m^2 and contact angle as 117° for both intrusion-de-pressurization cycles (33). Thus, Washburn equation becomes:

$$P(psi) = \frac{127.500}{D(\mu m)} \qquad \text{(Eq. 29)}$$

Winslow and Diamond (33) determined the contact angle of mercury on oven dried hardened cement pastes by observing the pentration pressure of mercury into small bore holes of known diameters. The assumption of equal contact angle in first and second intrusion is supported by Winslow and Diamond's procedure, since they intruded and withdrew mercury from the small holes in cycles and observed no change in penetration pressure.

The pore-size distributions of the agitated pastes are shown in Figure 13. Duplicate samples of air-entrained pastes were tested. The difference in the first intrusion total porosities indicate that the air contents of the two pastes were not the same. Despite this difference, the second intrusion curves were similar indicating the reproducibility of results. Hence, only one sample was tested to represent the 0.6/3d/AFx pastes.

The pore-size distributions of the unagitated pastes are shown in Figure 14. The air content of the particular 0.6/3d/A sample tested is very small, because there is little difference in the first intrusion total porosities of 0.6/3d/AF and 0.6/3d/A pastes. Comparing with the agitated pastes, it should not be concluded that little air can be entrained into unagitated pastes, but the observation should be regarded as an indication of the wide variation of the air content of individual

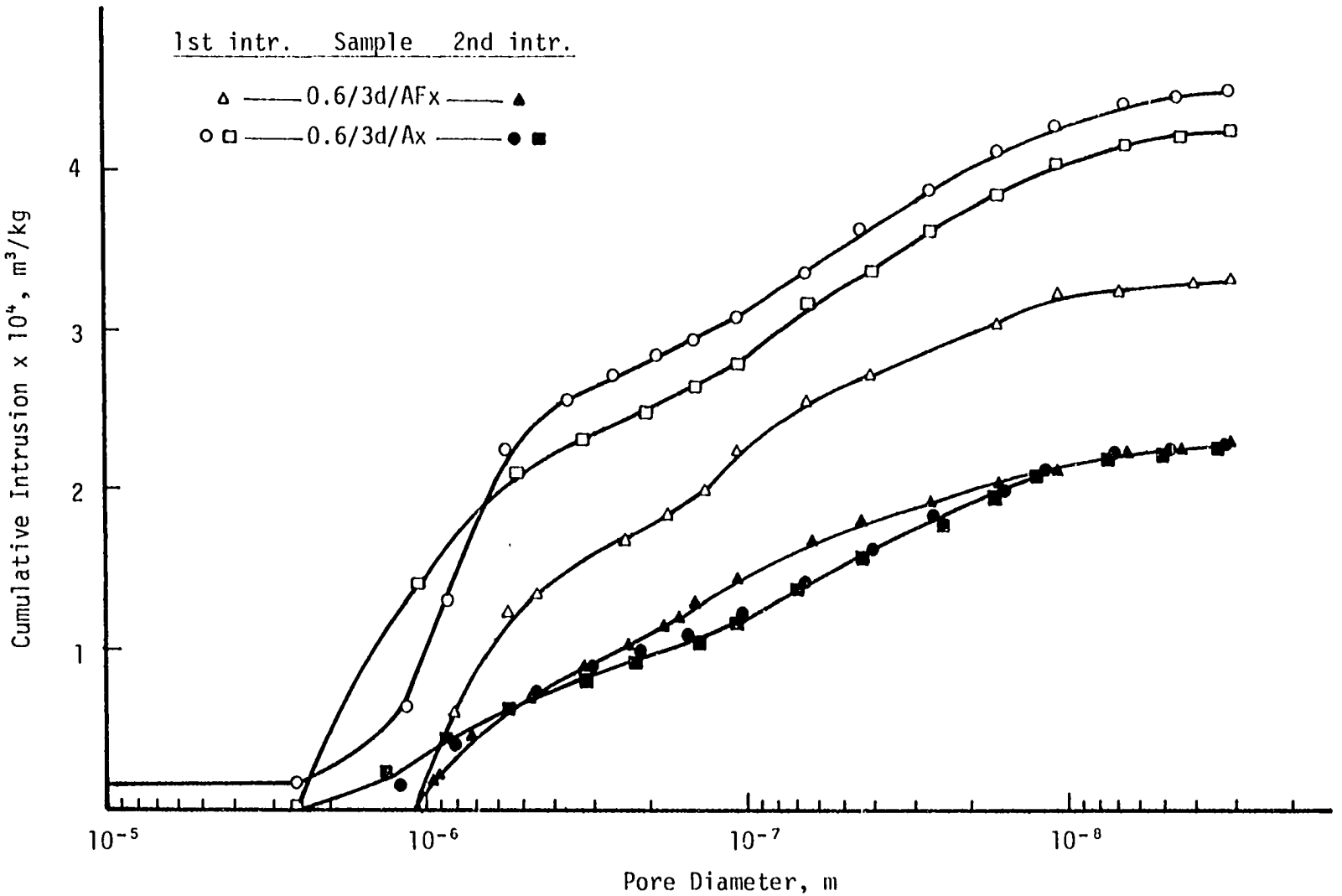

Figure 13. Pore-size distributions of agitated hardened cement pastes (W/C = 0.6, cured for 3 days)

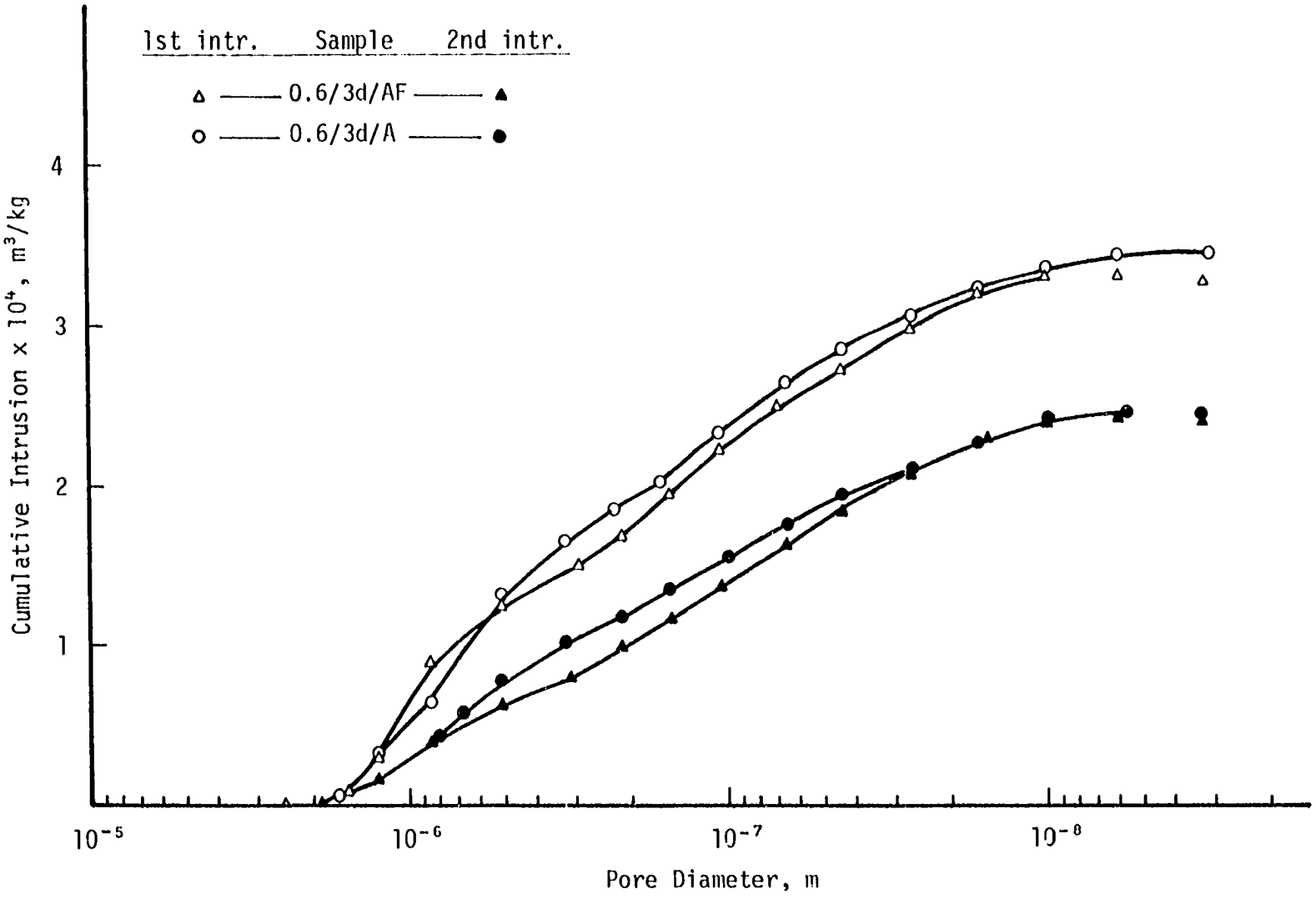

Figure 14. Pore-size distributions of hardened cement pastes (W/C = 0.6, cured for 3 days)

samples obtained from the same batch of paste. More evidence supporting this conclusion will be provided later.

The comparison of Figures 13 and 14 reveals many observations related to the first and second intrusion threshold diameters, pore-size distributions and total porosities of the different pastes. However at this point, only one aspect of the problem will be discussed in order to establish the sample preparation method. Does agitation influence the pore structure of hardened cement pastes? As discussed above, the first intrusion curves of air-entrained samples should not be used to answer this question. The comparison of the second intrusion curves of air-entrained samples and first and second intrusion curves of air-free samples shows that agitation during molding has caused a decrease in the total pore volume and a reduction in the pore sizes of hardened cement pastes. The extent of the variation in the pore structure may depend on the degree of agitation. Hence, if the paste must be agitated during molding, a standard procedure must be adopted instead of tapping the molds arbitrarily as described earlier. Standardization of the agitation procedure is not essential for this study, because the unagitated molding method may be accepted as a standard sample preparation technique. Thus, the conclusion of the first phase of investigations is that, if the cement pastes that will be examined in this study are prepared by mixing as described above and placed in the molds with a minimum amount of disturbance, different samples of the same batch will be consistent among themselves, and samples of different batches will be comparable with each other.

A portion of the 0.6 water-cement ratio pastes were replaced in the humidity room after breaking the tubes and vials at the end of 3 days of curing. A fraction of these pastes were cured for 28 days and the remaining for 60 days. Other batches of pastes were mixed with 0.4 and 0.5 water-cement ratios and cured for 3 days. All the hardened pastes were tested in the mercury intrusion porosimeter as described above. The physical characteristics and pore-size distributions of the hardened paste will be presented and discussed in the next chapter.

Preparation of Mortars

Mortar samples were mixed following ASTM test method C-305 with the exception that a larger size mixer was used; i.e., a Hobart Model N-100 instead of the Model N-50 mixer. A water-cement ratio of 0.49 produced a mortar of plastic consistency and an additional batch of mortar was mixed with a water-cement ratio of 0.6. The fresh mortars were placed in 2-inch cube molds, allowed to set in the humidity room, and then removed from the molds and cured for 60 days. At the end of the curing period the compressive strengths were determined following ASTM test method C-109. The compressive strengths are 3.44×10^7 N/m^2 (4990 psi) and 3.05×10^7 N/m^2 (4420 psi) for the 0.49 and 0.60 W/C ratio mortars, respectively.

In order to be able to compare the pore-size distribution of a mortar with the corresponding paste of equal water-cement ratio and age, the paste content of the mortar must be known. The determination of the weight fraction of sand in the mortar samples was performed as follows. Immediately after molding, the fresh mortar in one of the cubes was

removed and placed on a No. 100 sieve. The cement paste was washed through, and the sand remaining on the sieve was dried and weighed. This weight, divided by 0.98 to correct for the amount of sand that passes the No. 100 sieve, gives the weight of sand in a 1.31×10^{-4} m^3 (2 in^3) hardened mortar sample regardless of age. The oven-dry weight of 60 day old mortar cubes were determined, and the weight fraction of paste in mortar was calculated by the following formula:

$$\text{Paste Content} = \frac{\text{Dry wt. of mortar - Dry wt. of sand}}{\text{Dry wt. of mortar}}$$

The paste content of the mortar of normal consistency was determined to be 0.33. The 0.6 water-cement ratio mortar had a paste content of 0.31. Mortar samples were tested in the porosimeter similar to the pastes. The weight of oven-dry mortar samples tested in the porosimeter were multiplied by the paste contents for the calculations made to determine the pore-size distributions of the mortars per unit weight of paste.

RESULTS AND DISCUSSION

Mercury intrusion porosimetry has been used in the investigation of the pore-size distributions of hardened cement pastes (2,3,13,26,33). The purpose of the authors was to improve our understanding of the microstructure and behavior of hardened cement paste, mortar and concrete. Different aspects of the problem have been investigated on pastes prepared with various methods using different water-cement ratios, mixing procedures, curing conditions and periods (2,3,26,33). Mercury intrusion porosimetry results have been compared with pore-size distribution curves obtained by capillary condensation methods (11,21), and the discussions extended to the controversy over the microstructure of hardened cement pates (4,12,21). The amount of mercury retained in the samples upon depressurization was reported (2,26), but no previous investigations of second intrusion pore-size distributions of hardened cement pastes nor mercury intrusion porosimetry work on air-entrained cement pastes or mortars is known to the author.

Throughout this study, Washburn equation was used in converting the test data to pore-size distribution curves. One reason for making this choice, rather than using the equations derived for conical or spherical pores, is that Brunauer and associates concluded that cylindrical pore shape idealization gives better results than spherical geometry in evaluating capillary condensation data of hardened cement pastes (7). Thus, mercury intrusion porosimetry data were evaluated by Washburn equation, although pore sizes encountered in capillary condensation coincide only with the higher pressure ranges of pororimeter tests. The second reason

for using Washburn equation is that the results are used for comparative purposes in this study. If the pores in hardened cement pastes are conical with a characteristic α angle, the pore-size distributions will shift to larger pore sizes for all pastes; hence, the comparison will not be affected.

Hardened Cement Pastes

In order to investigate the effect of air-entraining on the pore structure of hardened cement pastes of various water-cement ratios and ages, the pastes shown in Table 3 were prepared by the procedures followed in preparing the 0.6/3d/AF and 0.6/3d/A pastes. The densities of the air-entrained pastes should be lower than the corresponding air-free pastes; however, the density of an individual sample depends on the air content of that sample. The densities and evaporable water contents of the air-entrained pastes are not reported in Table 3, because they vary from one sample to another within the same batch of paste. The evaporable water content, determined by evaporating the free moisture of samples at 105±5°C (22), is also called "water porosity" (2,3), because it corresponds to the total volume of water accommodated in the pores of the sample. The non-evaporable water, determined by igniting the pastes at 1050±10°C, gives an indication of the extent of hydration, because it corresponds to the amount of water of crystallization in the hydration products (22).

Table 3 shows that as the water-cement ratio decreases and age increases the density increases and evaporable water content decreases. High density and low evaporable water content indicate a less porous

Table 3. Physical characteristics of hardened cement pastes

Sample	Solid density (kg/m^3)	Evaporable water (kg/kg) dry paste	Nonevap. water (kg/kg) ignited paste
0.4/3d/AF	1580	0.25	0.12
0.4/3d/A	-	-	0.10
0.5/3d/AF	1390	0.33	0.13
0.5/3d/A	-	-	0.10
0.6/3d/AF	1250	0.39	0.14
0.6/3d/A	-	-	0.12
0.6/28d/AF	1350	0.36	0.19
0.6/28d/A	-	-	0.16
0.6/60d/AF	1470	0.33	0.25
0.6/60d/A	-	-	0.21

paste (27). At equal ages, the nonevaporable water contents of higher water-cement ratio pastes are greater, because the rate of hydration reactions is faster in the presence of a greater amount of water (6,17,27). At equal water-cement ratio, the increase in nonevaporable water content with increasing age is an indication of the continuation of the hydration reactions with time (6,17,27). The nonevaporable water contents of air-entrained pastes are less than those of the corresponding air-free pastes indicating that the air-entraining agent slows the rate of hydration reactions.

The pore size distributions of the hardened cement pastes listed in Table 3 are shown in Figures 14-18. It can be seen that the cumulative intrusion curves of some pastes tend to show a slight drop in total porosity beyond 0.01 x 10^{-6} m pore diameter as shown by discontinued lines

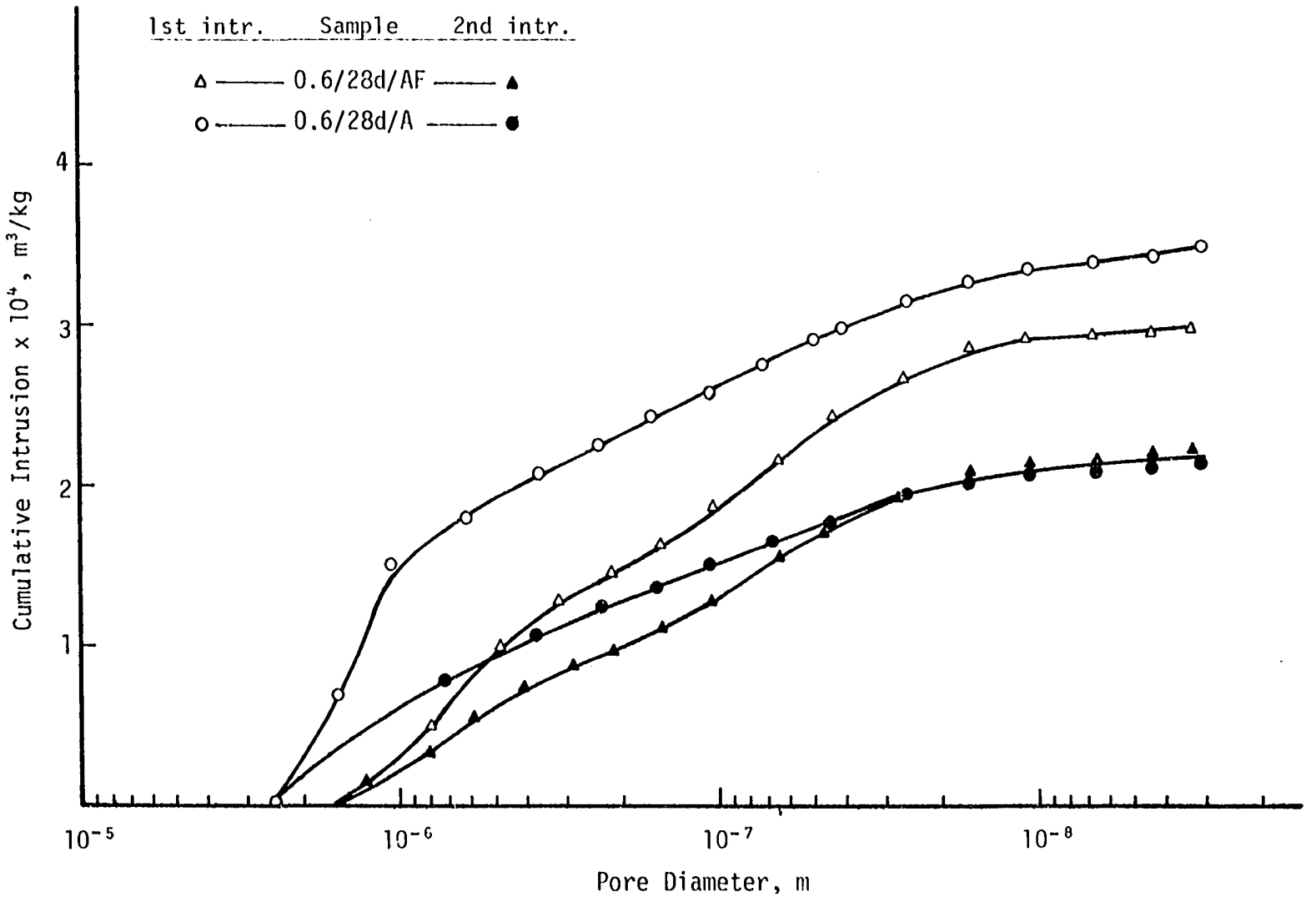

Figure 15. Pore-size distributions of hardened cement pastes (W/C = 0.6, cured for 28 days)

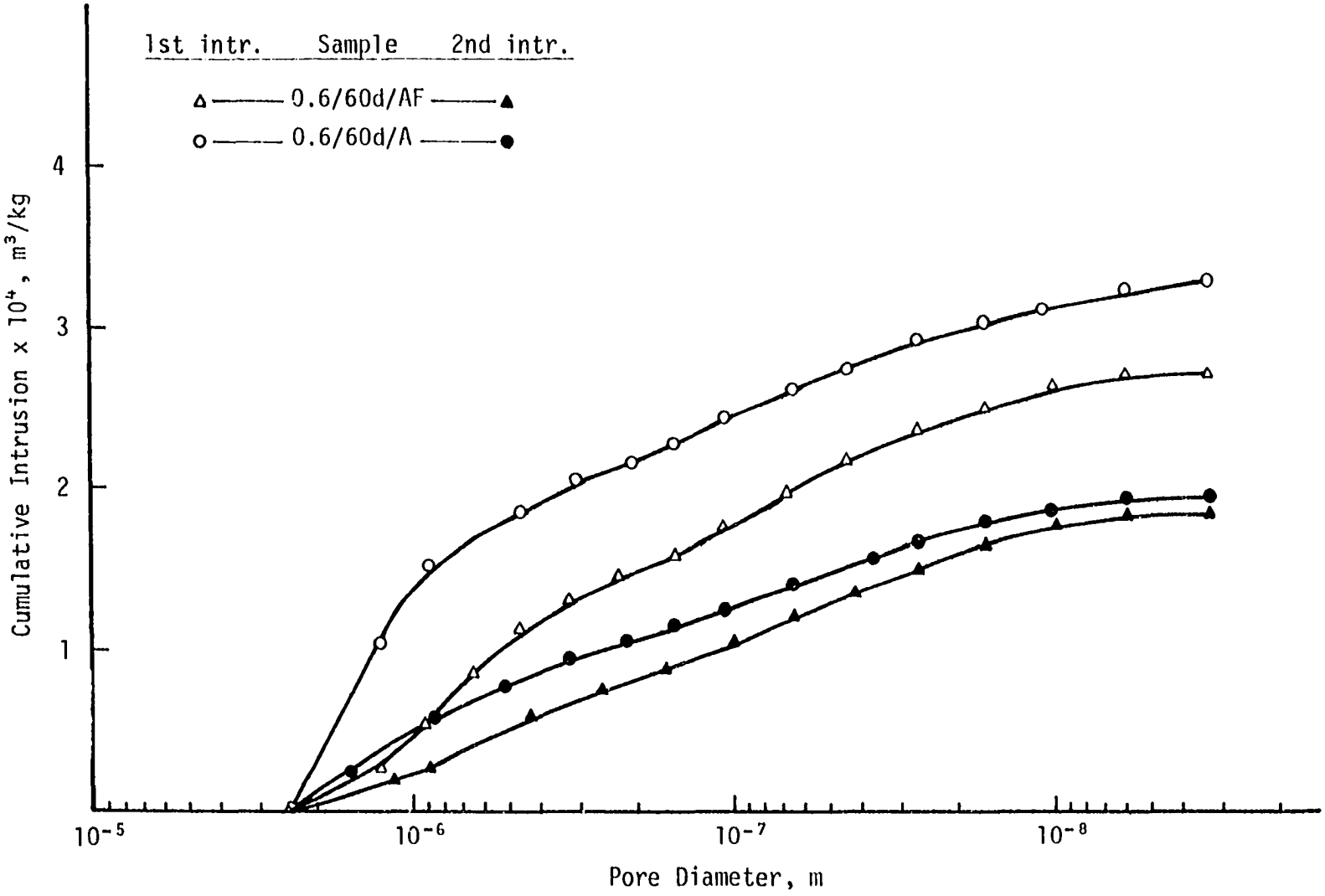

Figure 16. Pore-size distributions of hardened cement pastes (W/C = 0.6, cured for 60 days)

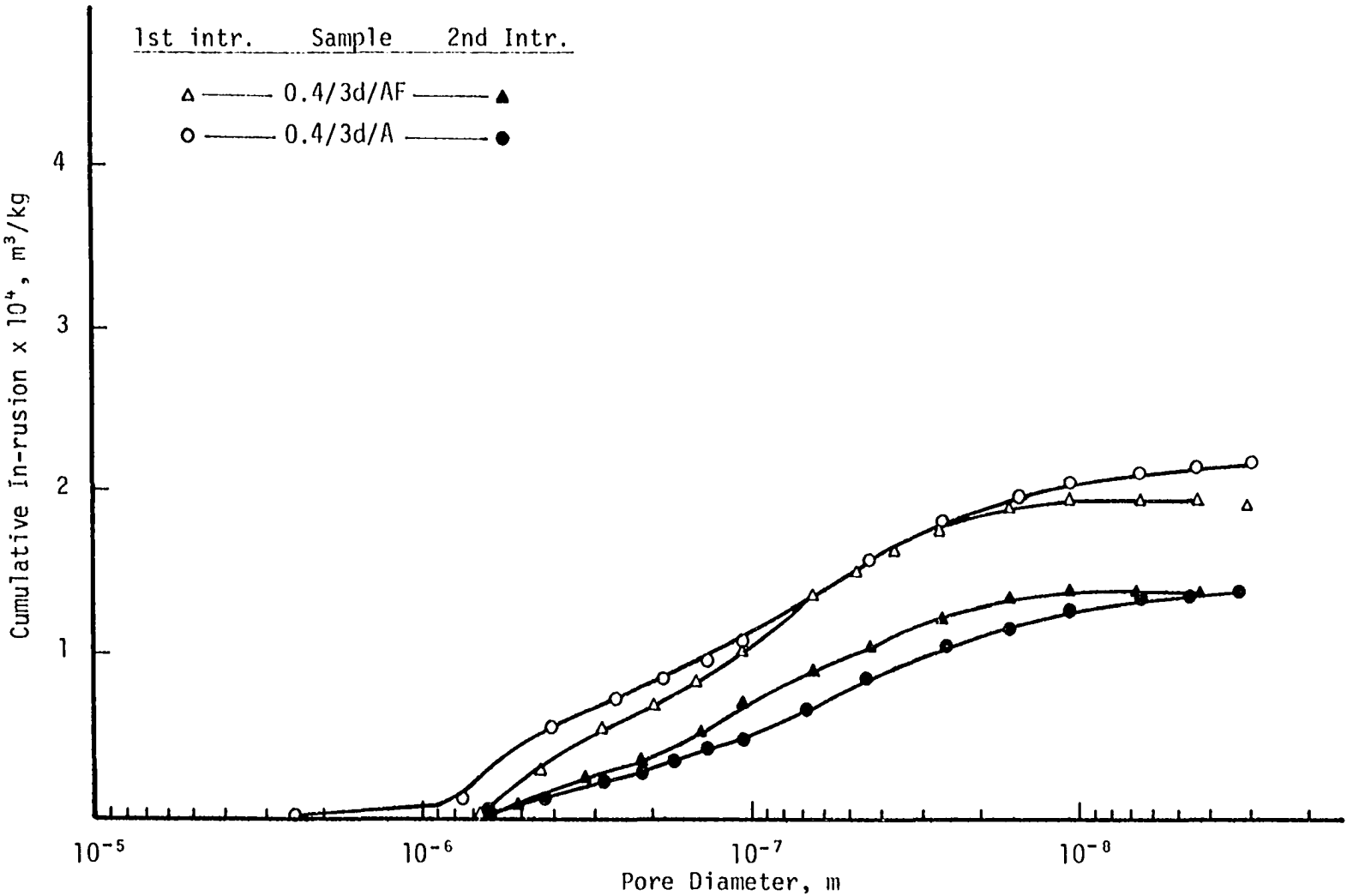

Figure 17. Pore-size distributions of hardened cement pastes (W/C = 0.4, cured for 3 days)

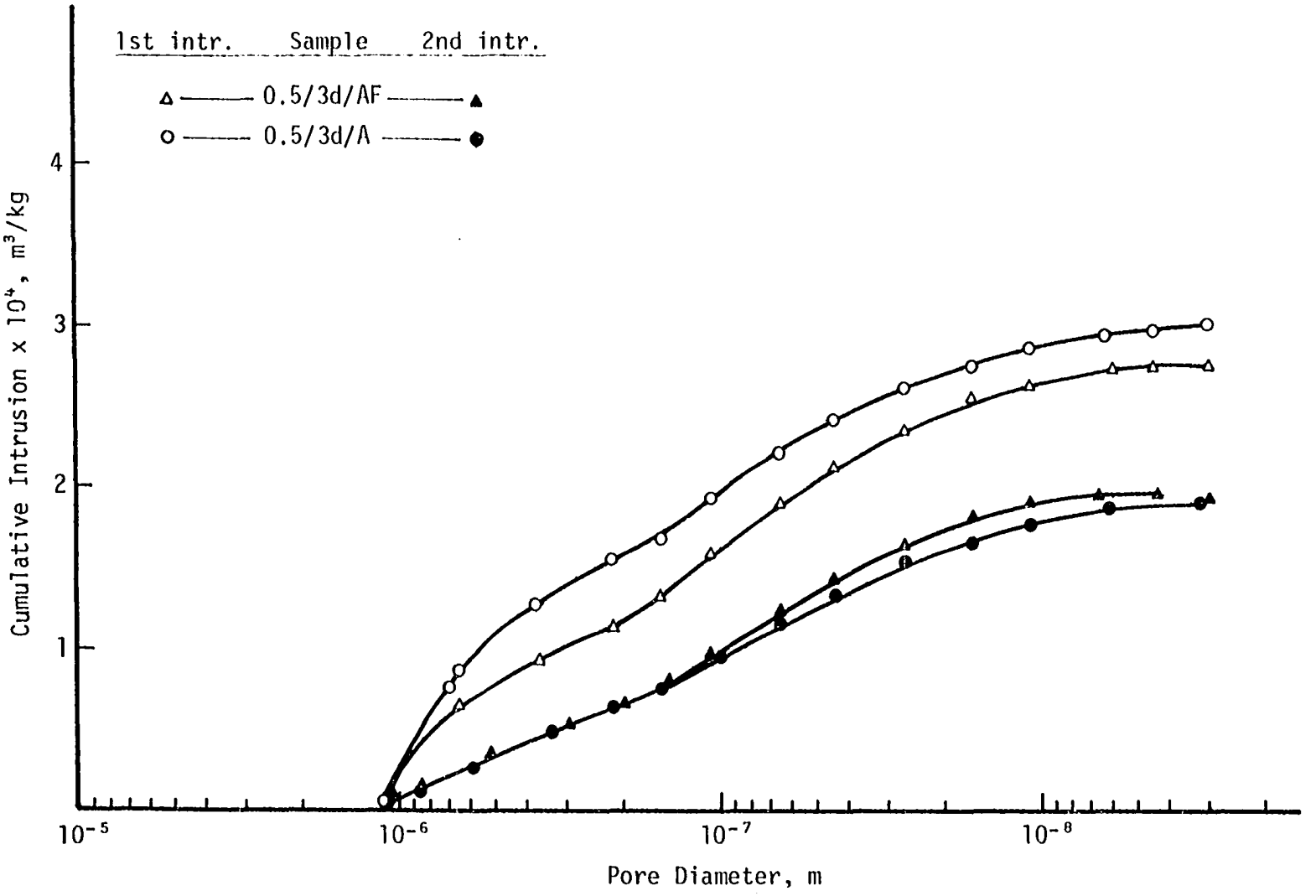

Figure 18. Pore-size distributions of hardened cement paste (W/C = 0.5, cured for 3 days)

in Figures 14, 17 and 18. Similar observations were made on mortar samples. Obviously, a decrease in cumulative intrusion has no physical meaning. In order to check if this was due to delayed completion of intrusion at high pressures, some samples were subjected to the maximum intrusion pressures for 5-6 hours. It was observed that equilibrium was reached within the initial 30 minutes and no further intrusion was recorded during the remaining period. Therefore, it was reasoned that this anomaly is due to the inadequacy of blank runs as the correction for the compressibility of the sample cell-mercury-sample system (18,25). Blank run data are obtained by applying the intrusion pressures on the sample cell filled only with mercury (25). If the compressibility of the sample is significantly smaller than the compressibility of mercury, the blank run overestimates the volume which is subtracted from the raw intrusion volume to compensate for the compressibility of the system. When the overestimation exceeds the intrusion into the sample, the cumulative intrusion tends to show a decrease.

The compressibility corrections for the sample cell used in this study were 6×10^{-9}, 27×10^{-9} and 61×10^{-9} m^3 at 8.96×10^7 N/m^2 (13,000 psi), 1.52×10^8 N/m^2 (22,000 psi) and 2.76×10^8 N/m^2 (40,000 psi), corresponding to 9.8×10^{-9}, 5.8×10^{-9} and 3.2×10^{-9} m pore diameters, respectively. The corrections were negligible at lower pressures corresponding to diameters larger than 0.01×10^{-6} m. The compressibility of mercury at maximum pressures applied in porosimeter tests is about 2.14×10^{-10} m^2/N (2.14×10^{-11} cm^2/dyne) (32), whereas the compressibility of concrete is 7.25×10^{-11} m^2/N (7.25×10^{-12} cm^2/dyne) as

calculated from an average modulus of elasticity (29). The mortar samples contain large fractions of Ottawa sand for which the compressibility may be taken from data on quartz (29) as 3.22×10^{-12} m^2/N (3.22×10^{-13} cm^2/dyne). It is seen that compressibilities of concrete and quartz are approximately 50 and 200 times smaller than that of mercury, respectively. The difference between a blank run and a test with a sample in the cell is that a volume of mercury equal to the volume occupied by the sample is replaced by a sample 50 or 200 times less compressible than mercury. This difference accounts for the apparent decrease in cumulative intrusion observed in some tests above 8.96×10^7 N/m^2 (13,000 psi). All the pore-size distribution curves of the pastes and mortars may underestimate the cumulative intrusions above 8.96×10^7 N/m^2 (13,000 psi), but the exact amount of underestimation depends on the size and compressibility of the sample in each case.

The major conclusions of earlier investigations of pore-size distributions of hardened cement pastes were mentioned in the beginning of methods of investigation. Those observations were made on the first intrusion pore-size distribution curves of hardened cement pastes only and do not cover second intrusion curves nor pore structure analysis of air-entrained pastes or mortars. In this study, before the analysis of second intrusion curves and pore-size distribution of air-entrained pastes, the first intrusion curves of air-free pastes will be compared with the results of Winslow and Diamond (33) as shown in Table 4.

The 0.6 water-cement ratio pastes prepared in this study are more porous than those prepared by Winslow and Diamond (33). The difference in

Table 4. Comparison of pore volume data

Sample	Prepared and tested in	Degree of hydration %	Water porosity 10^{-6} m^3/kg	Cumulative intrusion at $8x10^{-9}m$ pore diameter $10^{-6}m^3/kg$
0.6/3d/AF	This study	-	394	331
0.6/3d/AF	Ref. 33	53.2	373	300
0.6/28d/AF	This study	-	362	295
0.6/28d/AF	Ref. 33	76.5	337	226
0.6/60d/AF	This study	-	331	267
0.6/59d/AF	Ref. 33	80.7	323	204

cumulative intrusion increases from 31 x 10^{-6} m^3/kg to 69 m^3/kg when the age increases from 3 to 28 days, and then drops to 63 m^3/kg when the ages of the pastes are 59 or 60 days. This trend can best be explained by the different curing methods rather than the different mixing and molding procedures, although the latter must be responsible for the different porosities of 3 day old pastes since the difference drops to 21 m^3/kg when the 0.6/3d/AFx paste shown in Figure 13 is compared with Winslow and Diamond's data. Winslow and Diamond immersed their pastes into saturated calcium hydroxide solution, whereas a humidity room was used for this study. The reason for this choice was that an excessive accumulation of calcium hydroxide crystals was observed by scanning electron microscope in the air voids of air-entrained pastes as shown in Figure 10. Figures 10b and d show that a small amount of calcium hydroxide deposition is observed in the air voids of pastes cured in humidity room or immersed in water. Comparison of Figures 10a and c indicate considerable growth of crystals with

longer curing periods. There was no evidence of any influence of the calcium hydroxide deposits on the mercury intrusion porosimetry results, but the pastes in this study were cured in the humidity room where the conditions are more similar to the environment of the cement paste in constructions. However, the relative humidity maintained during curing was lower than 100 percent, therefore the pastes cured in the humidity room hydrated slower than those cured in calcium hydroxide solution (22). This would cause an increase in the difference between the porosities of 28 day old pastes as compared to the difference between 3 day old pastes. The rate of hydration reactions slows down as the degree of hydration increases with time as clearly seen in Table 4 for Winslow and Diamond's pastes. The degrees of hydration were not determined in this study, but due to lower relative humidity during curing, they would be lower than those reported for similar pastes by Winslow and Diamond. Hence, during the period between 28 and 60 days, the hydration in these pastes will not slow down as much as the hydration slows down in Winslow and Diamond's pastes, thereby causing a decrease in the difference between the porosities of 60 day old pastes.

It is also seen in Table 4 that the differences between the water porosities, or total pore volumes of the pastes prepared for this study and by Winslow and Diamond are smaller than the differences between the cumulative intrusions, i.e., the differences between the corresponding pastes shown in the fourth column are smaller as compared with the differences in the last column. Hence, the different methods of mixing and curing affect total porosity less than the porosity in the pores greater

than 8 x 10^{-9} m diameter. This is another demonstration of the influence of the sample preparation procedure on the pore-size distributions of hardened cement pastes.

The above comparison shows that the pore-size distribution curves obtained in this study are not exactly the same as those reported by Winslow and Diamond (33). However, the general concept that "as a paste hydrates the total pore volume decreases and a general reduction in pore size takes place" (33) is confirmed by Figures 14-16. The same trend is observed with decreasing water-cement ratio in Figures 17, 18 and 14. The results of this study confirm the existence of a threshold diameter and its decrease with decreasing water-cement ratio. It should be mentioned that in the agitated pastes shown in Figure 13, the threshold diameter is well-defined with a sharp increase in the cumulative intrusion after its intrusion. In case of unagitated pastes shown in Figures 14-18, the sharp increase in cumulative intrusion after the intrusion of the threshold diameter is smaller as compared to the agitated pastes. Hence, Bager and Sellevold's observation that, "the threshold diameter is extremely sensitive to the exact details of the specimen preparation" (3) is confirmed in this study. Consequently, it may be stated that the first intrusion pore-size distribution curves of the air-free hardened cement pastes of this study conform to the results of earlier investigations.

The uniform pore-size distributions of hardened cement pastes were determined by the second intrusion method. The second intrusion curves are plotted on the same figures with the first intrusion curves, as shown in Figures 13-18. It is seen that the uniform pore-size distribution of

the pastes have similar characteristics as the first intrusion curves; i.e., with increasing age and decreasing water-cement ratio the total uniform pore volume decreases and a general reduction in uniform pore size takes place. The second intrusion threshold diameter is equal to or smaller than the first intrusion threshold diameter. The major fraction of the difference between the total and uniform pore volumes is within a short range of pore diameters slightly smaller than the threshold diameter, which means that a large volume of ink-bottle pores have entrances in this range. The diameter of the ink-bottle pores may be much larger than the entrances; hence, it would be incorrect to state that an air-free hardened cement paste does not contain pores of sizes greater than the threshold diameter. The implications of this conclusion may be better visualized by a reference to the hypothetical specimens discussed earlier. The incremental difference between the first and second intrusion curves decreases as smaller pores are intruded which means that there is a greater volume of ink-bottle pores communicating with the outside through the pores slightly smaller than the threshold diameter. Due to the limitations of the second intrusion method the size or number of ink-bottle pores cannot be determined. As an example of the above statements, the first and second intrusion curves of 0.6/3d/AFx paste shown in Figure 13 can be analyzed. The threshold diameter of both intrusions is 10^{-6} m. There are 60 x 10^{-6} m^3/kg ink-bottle pores with entrances in the range of 10^{-6} - 0.5 x 10^{-6} m. The diameters of the ink-bottle pores may be greater than 10^{-6} m. If the pores are assumed to be cylindrical the diameters of the ink-bottles must be at least twice the diameters of the entrances,

i.e., $2 \times 10^{-6} - 10^{-6}$ m. The volumes of ink-bottle pores with entrances in the range 5×10^{-7}-10^{-7} m and $10^{-7} - 10^{-8}$ m are both 20×10^{-6} m^3/kg which shows the decrease in the volume of ink-bottles communicating with the outside through narrower entrances.

The difference between the total intrusion volumes of the first and second intrusions is equivalent to what has been reported by others as the amount of mercury retained at the end of de-pressurization and is a measure of total volume of ink-bottle pores. Table 5 shows the total pore volume from the first and second intrusion of mercury into hardened cement pastes. The retention factor expressed in the last column is the volume percentage of ink-bottle pores based on the first intrusion total porosity. The ink-bottle pores in air-free pastes constitute between 25 to 31.4 percent of the total pore volume but it is difficult to observe a trend in the variation of retention factor with water-cement ratio and age of the pastes. Sellevold (26) found the retention factor to be between 20 and 45 percent on mature pastes mixed in vacuum with 0.35 and 0.45 water-cement ratios. Auskern and Horn (2) predicted an increase in the retention factor with the degree of hydration, but their pastes were prepared under atmospheric pressure. The results of this study reveal that entrapped air cannot be eliminated under such conditions. Thus, it is more likely that the pastes tested by Auskern and Horn contained some air voids that cannot be filled by hydration products even in mature pastes. Since the total porosity of hardened cement pastes decreases with increasing hydration, the volume of mercury retained in the air voids will be more pronounced when compared with the decreased total porosity. Hence, the

Table 5. Comparison of total uniform and ink-bottle pores

Sample	Total volume intruded (10^{-6} m^3/kg) First intrusion	Second intrusion	Retention factor
0.4/3d/AF	196	139	29.1
0.4/3d/A	219	138	37.0
0.5/3d/AF	265	196	26.0
0.5/3d/A	301	190	36.9
0.6/3d/AF	332	244	26.5
0.6/3d/A	344	248	27.9
0.6/3d/AFx	333	231	30.6
0.6/3d/Ax	451	227	49.7
0.6/3d/Ax	424	225	46.9
0.6/28d/AF	300	225	25.0
0.6/28d/A	351	214	39.0
0.6/60d/AF	271	186	31.4
0.6/60d/A	320	197	38.4

prediction made by Auskern and Horn (2) should not be directly applied to pastes mixed under evacuation.

Obviously, the retention factors of air-entrained pastes are always greater than the corresponding air-free samples as seen in Table 5. The retention factor varies considerably from one paste to another due to the different air contents.

The most important observation concerning the pore structure of air-entrained hardened cement pastes is achieved by a comparison of the second intrusion curves of such pastes with the corresponding air-free samples. Table 5 shows that the total second intrusion volumes of corresponding

air-entrained and no-air pastes agree within $\pm 11 \times 10^{-6}$ m^3/kg which means that air-entraining agent makes no systematic change in the uniform porosity of hardened cement paste. Hence, air-entraining introduces mainly large air voids in hardened cement pastes and does not affect the characteristic porosity observed in pastes containing no entrained or entrapped air. In other words, if an air-free paste contains x m^3/kg uniform pores and y m^3/kg ink-bottle pores, the corresponding air-entrained paste also contains x m^3/kg uniform pores as revealed by similar second intrusion curves. Thus the air-entrained paste must also contain y m^3/kg ink-bottle pores similar to the air-free paste and an additional z m^3/kg air voids introduced by the air-entraining agent. Obviously, the difference between the first intrusion curves of corresponding air-free and air entrained pastes must be equal to z m^3/kg.

It is seen in Figures 13-17 that the second intrusion pore-size distributions of air-free pastes with 0.4 and 0.5 water-cement ratios indicate slightly larger pore sizes than the corresponding air-entrained pastes, whereas the reverse is true for the 0.6 water-cement ratio pastes of three different ages. Therefore, with increasing water-cement ratio, the uniform porosity of air-entrained pastes is distributed slightly toward larger pore sizes as compared with the air-free pastes.

A fracture surface of an air-entrained sample is shown in Figure 9, where it is seen that the air voids have been intruded and the mercury was retained at the end of de-pressurization. What is more important is that mercury is not ejected from the large spherical air voids even when they have been broken open. An impact was applied on the sample when

breaking, but it was insufficient to eject the mercury from the voids. The broken sample was shaken, with the fracture surface facing down, but the effect of gravity and shaking was insufficient to eject mercury from the voids. The mercury in the spherical air voids could be ejected only after hitting the sample on the bench. This phenomenon is an experimental evidence of the theoretical statement that suction must be applied in order to withdraw mercury from a spherical pore.

Mortars

The pore-size distributions of the mortars were determined as shown in Figures 19 and 20. As mentioned earlier, the weight of the mortar samples is corrected for the sand content which is nonporous. Hence, in this study, the pore volume of mortar is always "based on the paste content"; e.g., the total first intrusion porosity of the mortar of plastic consistency is 316 x 10^{-6} m^3/kg of paste. The main idea behind the approach was to compare the pore-size distribution of mortar based on the paste content with the pore-size distribution of a similar pure paste. Therefore the pore size distribution of 0.5/60d/A paste was also determined as shown in Figure 21. The 0.6 water-cement ratio can be compared with the corresponding 0.6/60d/A paste shown in Figure 16.

It is difficult to compare the first intrusion curves since the air content of pastes and mortars may not be equal, and depending on the sand-paste ratio, mortars may have intergranular voids between sand particles coated with paste (9). However, these voids are in the ink-bottle category because they are interconnected by the characteristic fine pores of

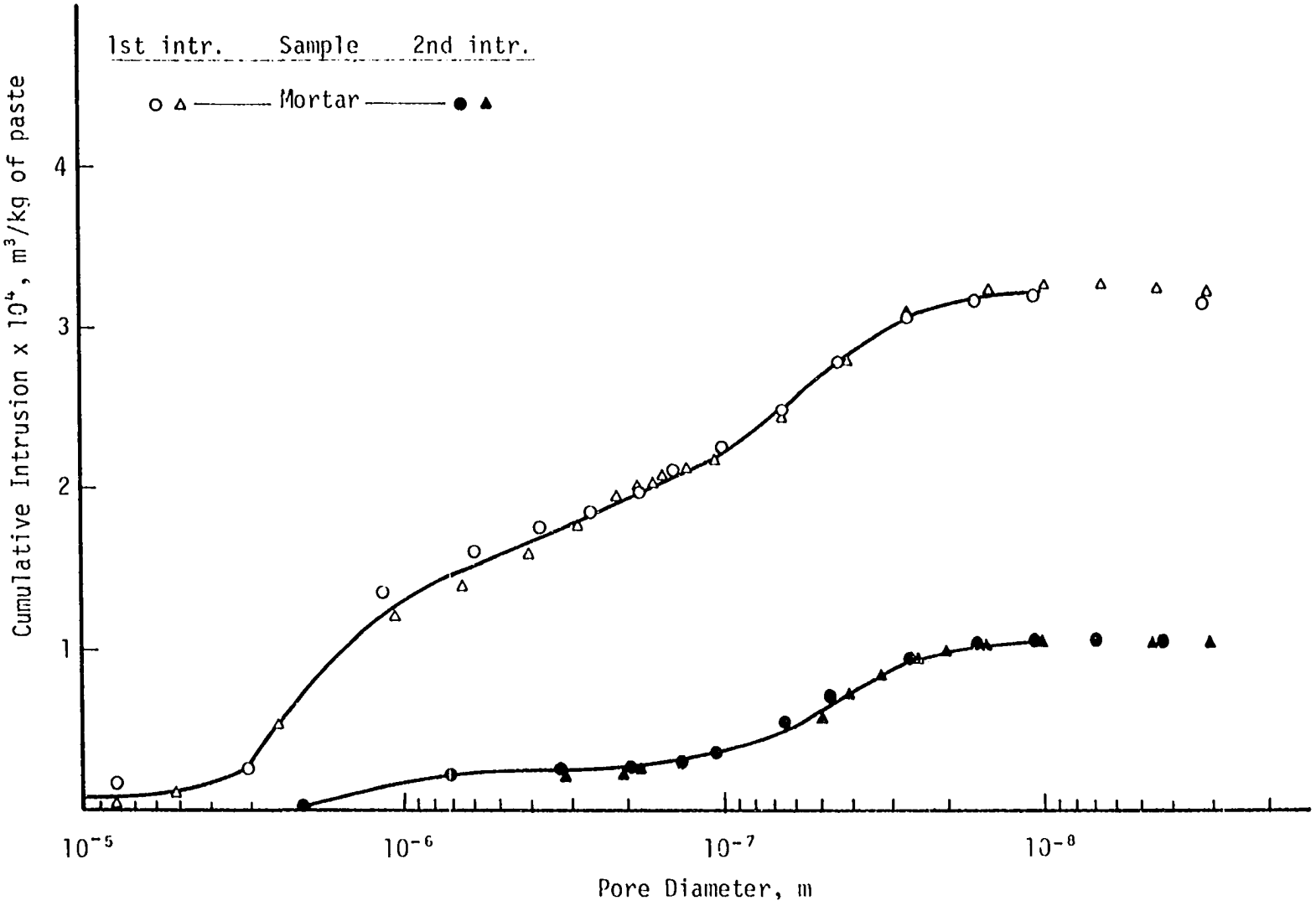

Figure 19. Pore size distribution of mortar (W/C - 0.49, cured for 60 days)

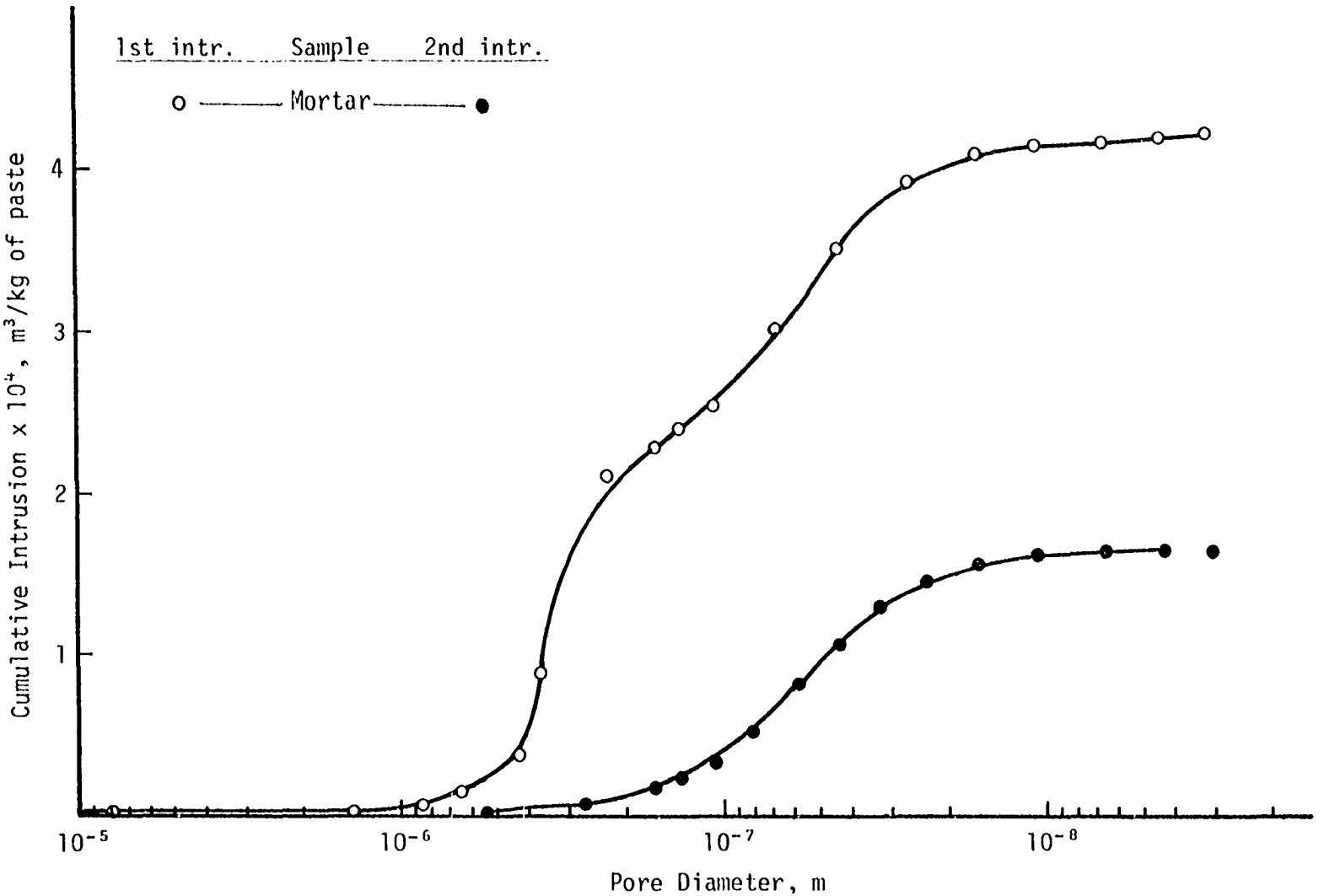

Figure 20. Pore-size distribution of mortar (W/C = 0.6, cured for 60 days)

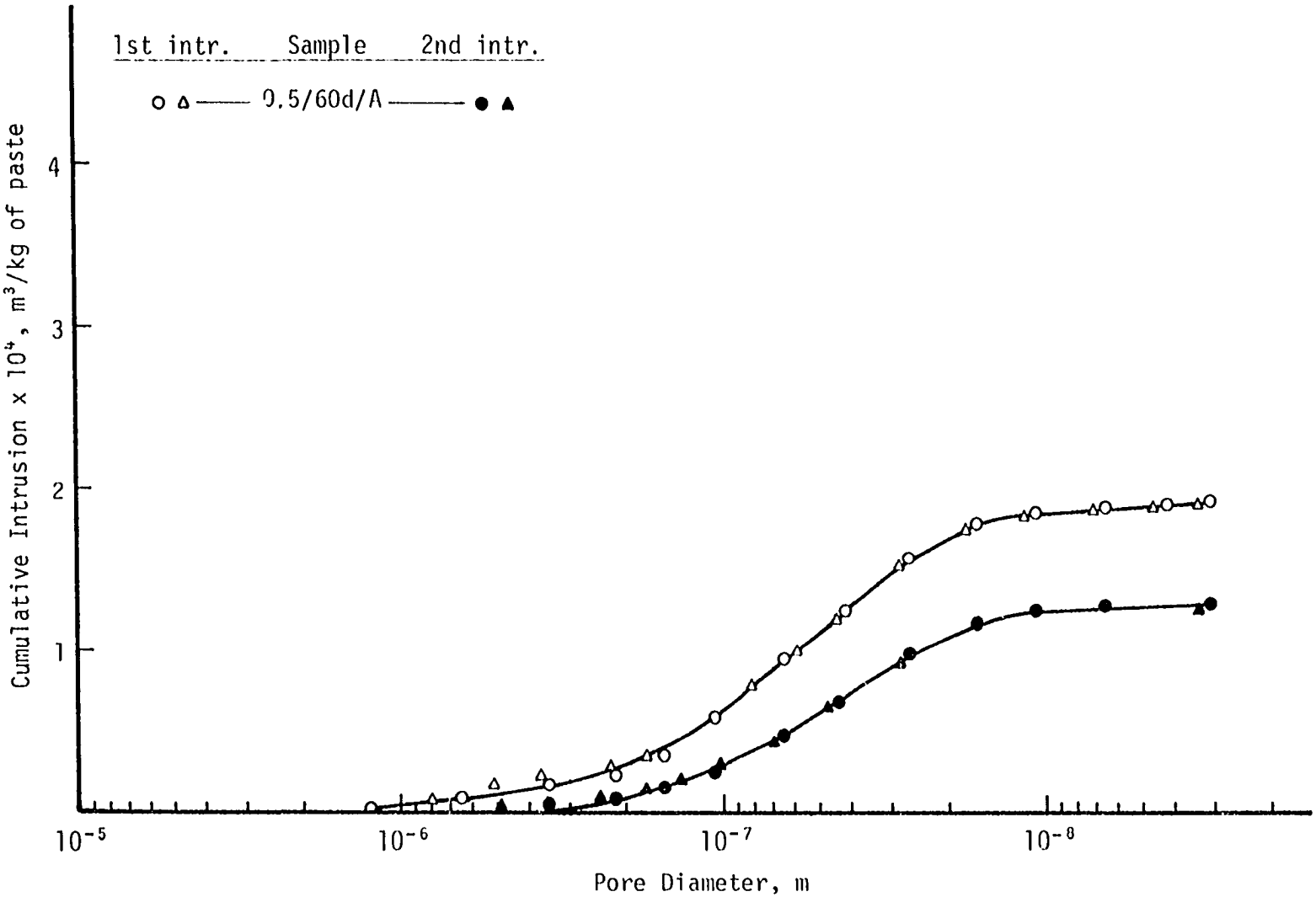

Figure 21. Pore-size distribution of hardened cement paste (W/C = 0.5, cured for 60 days)

the paste. Hence, they will retain mercury at the end of first intrusion and de-pressurization cycle. Consequently, the second intrusion curves of mortars are not influenced by the air voids and intergranular porosity, thus can be compared with the second intrusion curves of similar pastes.

The pore-size distribution of the mortar of plastic consistency with a water-cement ratio of 0.49 can be compared with the pore-size distribution of 0.5/60d/A paste since the effect of the small difference in the water-cement ratios is negligible. The first intrusion curves indicate that the mortar has a greater volume of larger pores per unit weight of paste, in the region of 5×10^{-6} to 0.5×10^{-6} m diameter after which the pore-size distribution is similar to that of the pure paste. The difference can be attributed to the intergranular porosity since the sand used in the preparation of the mortar was composed of uniform size particles which leave a greater amount of voids than well-graded particles.

The agreement between the second intrusion porosities is very good. The slightly smaller total intrusion of the mortar per unit weight of paste content can be explained by the fact that it was agitated and compacted during molding. Comparison of Figures 16 and 20 shows that the pore-size distributions of 0.6 water-cement ratio paste and mortar have similar trends as 0.5 water-cement ratio paste and 0.49 water-cement ratio mortar; i.e., the first intrusion porosity of the mortar per unit weight of paste is considerably higher than the pure paste, whereas the second intrusion porosity of the pure paste is lower than that of the mortar. However, the mortar can also be compared with a similar paste which has undergone agitation during molding. Thus, the pore-size

distribution of 0.6/60d/Ax paste was determined in the mercury intrusion porosimeter. The result is shown in Figure 22. Comparison of Figures 20 and 22 shows that the first intrusion curves do not match, but the second intrusion total porosities of the mortar per unit weight of paste content and the corresponding agitated paste are equal. Hence, it may be concluded that the second intrusion porosities of hardened cement pastes and mortars per unit weight of paste content will be equal if they are mixed and cured by a similar technique.

Figures 19 and 21 show that in 0.49 water-cement ratio mortar a relatively greater volume is allocated to larger pores as compared with the 0.5/60d/A paste. The reverse of this case is observed in Figures 16, 18 and 22 for 0.6 water-cement ratio pastes and mortar. This trend may be explained by the different paste-sand ratios in the two cases. In the mortar of plastic consistency, there is a smaller volume of paste to fill the voids between the sand particles so that the excess water can be accommodated in larger pores. However, in 0.6 water-cement ratio mortar, the volume of paste is greater so that during compaction the sand particles force the excess water to be dispersed into smaller pores. The amount of excess water is determined by the water-cement ratio and the stoichiometry of the hydration reactions. Therefore, the total second intrusion porosities of the pure pastes and mortars per unit weight of paste are equal regardless of how the excess water is accommodated. It should also be noted that threshold diameter of the 0.6 water-cement ratio mortar is smaller than the threshold diameter of the 0.49 water-cement ratio mortar for both the first and second intrusions. This observation

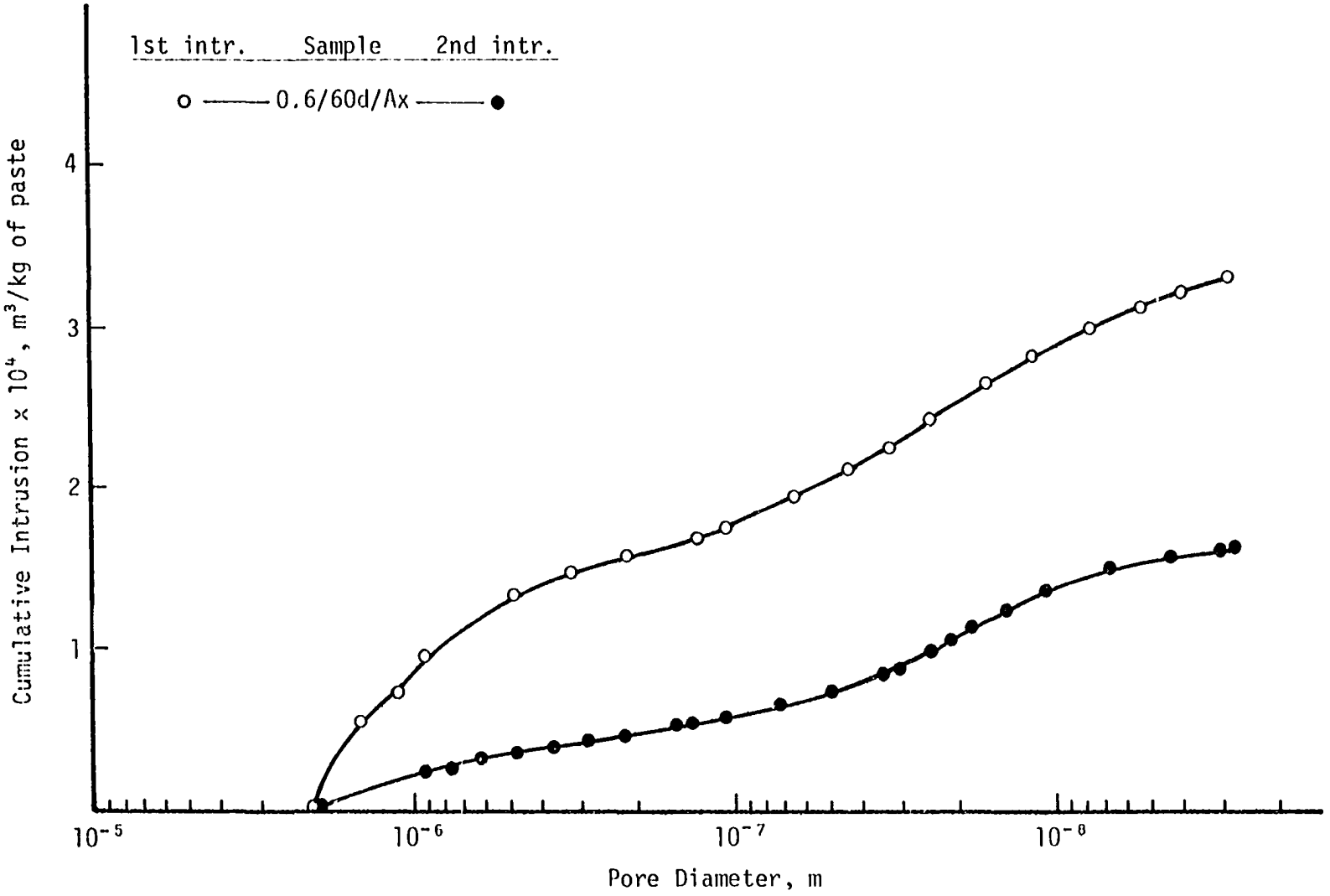

Figure 22. Pore-size distribution of agitated hardened cement paste (W/C = 0.6, cured for 60 days)

may also be accounted for by the above explanation. Similar observations were made in a previous study by this author where the mean pore radii of mortar of various water-cement and sand-cement ratios were determined (8).

Concrete

The preparation and testing of concrete samples is beyond the scope of this study; however, a discussion of possible applications of the results to concrete is undertaken here, because it is the most common building and structural material encountered by practicing engineers.

The importance of sample preparation technique has been emphasized several times in the present study and in other investigations. It is necessary to standardize a sample preparation method which will produce hardened cement pastes representative of the paste in the concrete mixed in plants and placed in construction sites. It should be clear that simply duplicating the water-cement ratios and curing periods does not reproduce identical pastes; mixing and placing procedures and curing conditions play an important role in obtaining representative samples. During mixing and molding the pure pastes must be agitated and/or vibrated in such a way that the compaction applied on the paste around the aggregate particles must be equally experienced by the pure paste prepared in the laboratory. The determination of this compaction energy and method is a separate research problem.

The second step in the standardization of sample preparation method is curing the paste under conditions similar to that experienced by the concrete in structures. This is difficult to establish due to the effect

of different curing practices and prevailing climates at various construction sites. Nevertheless, the effect of small differences in curing conditions will decrease as curing period increases since cement paste within ordinary Portland cement concrete is normally in equilibrium with an internal environment of high relative humidity, even under conditions that cause the surface of the concrete to dry substantially (34).

The effect of cement type on the pore-size distributions of hardened cement pastes should also be determined. The difference of sources supplying the cement or variation of composition within the same type of Portland cement should not alter the pore-size distributions considerably. The aggregate used in concrete production may not be a nonporous material, however, it should not be difficult to isolate and determine the porosity of some representative aggregate particles for the concrete sample.

Obviously, the paste content of hardened concrete must be determined in order to make corrections for aggregate content and porosity so that the pore-size distribution of the paste in concrete can be compared with the pore-size distribution of pure paste. The exact paste content of the samples tested in the porosimeter must be known; because due to the small sample size, the average paste content of a block of concrete may not represent the paste content of an individual porosimeter sample. The pore-size distribution curve will shift to higher or lower cumulative intrusions if the paste content of the sample is under or overestimated. This question also represents a research problem, because it is beyond the scope of ASTM test method C 85 for the determination of cement content of hardened Portland cement concrete.

A set of data similar to a calibration chart should be obtained when the pore-size distributions of the representative paste samples of various water-cement ratios and ages are determined. Then, any hardened concrete sample with a known age, paste content and aggregate porosity can be tested in the mercury intrusion porosimeter and the second intrusion porosity can be related to one of the standard pastes prepared in the laboratory. As long as the preparation and curing methods are similar, the concrete sample must have the same water-cement ratio with the hardened cement paste which shows the same second intrusion total porosity with the concrete sample. It is known that inadequate water-cement ratio may cause the failure of a concrete structure but there is no method to determine the water-cement ratio of hardened concrete. Hence, the above procedure may serve a very important purpose in concrete technology.

SUMMARY AND CONCLUSIONS

The purpose of this study was to improve mercury intrusion porosimetry testing and interpretation methods in order to gain more information about the pore structure of materials.

The review of mercury intrusion porosimetry theory showed that pore size and intrusion pressure can be related to each other by establishing the energy balance involved or solving the pressure differential across mercury meniscus. The relationship derived for the intrusion of conical and spherical pores is given by Equation 13:

$$\frac{P}{\gamma_{l,v}} r = -2 \sin(\theta+\alpha)$$

If a sample contains conical pores, the pore sizes calculated by Washburn equation are larger than the actual sizes. In case of spherical geometry, depending on the size of the entrance, the pore size distribution curve may result in larger or smaller sizes than the actual pores of the sample.

If mercury meniscus exists in a pore at the end of intrusion or if the pore has a slit-like shape, the withdrawal of mercury must follow the intrusion equations. However, mercury in a completely intruded uniform cylindrical or prismatic pore of a given size is ejected at a lower pressure than the intrusion pressure, whereas the main portion of ink-bottle pores, gently sloping conical pores, and spherical pores retain mercury at the end of de-pressurization. Hence, the uniform pore-size distribution of a sample can be determined by intruding the sample a second time because the ink-bottle pores have no influence on the second intrusion. The second intrusion curve also indicates the volume of ink-bottle pores intruded at each entrance diameter.

Investigations of the pore structure of air-entrained cement paste and mortar utilized the improved mercury intrusion porosimetry interpretations. The analyses led to the following conclusions:

1. Sample preparation technique affects the pore size distribution of hardened cement pastes. In order to obtain consistent and comparable results in different studies, the mixing, molding and curing procedures must be standardized.

2. Similar to the first intrusion, the second intrusion pore-size distributions of hardened cement pastes shows a decrease in total uniform pore volume and a reduction in uniform pore size with increasing age and decreasing water-cement ratio.

3. Approximately two-thirds of the total intrusion volume of an air-free paste is due to uniform pores and the remaining to ink-bottle pores. The major fraction of the total volume of ink-bottle pores is intruded through entrances of sizes slightly smaller than the threshold diameter.

4. The second intrusion curves of air-entrained hardened cement pastes containing different amounts of air match with the second intrusion curves of corresponding air-free pastes. Therefore, air-entraining only introduces the large air voids seen in Figure 9, and does not alter the finer pore structure of hardened cement paste appreciably.

5. The second intrusion total porosity of the mortars compares favorably with the second intrusion porosity of air-entrained pastes provided that similar preparation techniques are used and the porosity of mortar is expressed as the volume of pores per unit weight of the paste content. The pores in mortar are distributed as smaller sizes than the

pure pastes. This is thought to be the result of compaction applied by the sand particles.

The results indicate that the water-cement ratio of hardened concrete may be estimated if a comparison chart is prepared by determining the second intrusion pore-size distributions of standard hardened cement pastes. This topic is recommended for further research.

REFERENCES

1. Adamson, A. W. 1967. Physical chemistry of surfaces. Interscience Publishers, Inc., New York.

2. Auskern, A. and W. Horn. 1973. Capillary porosity in hardened cement paste. JTEVA 1: 74-79.

3. Bager, D. H. and E. J. Sellevold. 1975. Mercury porosimetry of hardened cement paste: The influence of particle size. Cem. Conc. Res. 5: 171-178.

4. Beaudoin, J. J. 1972. A discussion of the paper by S. Diamond. Cem. Conc. Res. 2: 146-147.

5. Bogue, R. H. 1955. The chemistry of portland cement. 2nd ed. Reinhold Publishing Co., New York.

6. Brunauer, S. and L. E. Copeland. 1964. The chemistry of concrete. Sci. Am. 210(4): 81-92.

7. Brunauer, S., R. Sh. Mikhail, and E. E. Bodor. 1967. Some remarks about capillary condensation and pore structure analysis. J. Colloid Interface Sci. 25: 353-358.

8. Caro, J. H. and H. P. Freeman. 1961. Pore structure of phosphate rock and triple superphosphate. Ag. Food Chem. 9: 182-186.

9. Cebeci, Ö. Z. 1974. A simple method to determine pore radius of mortar. M.S. thesis. Middle East Technical University, Ankara, Turkey.

10. DeWit, L. A. and J. J. F. Scholten. 1975. Studies on pore structure of adsorbents and catalysts. J. Catal. 36: 36-47.

11. Diamond, S. 1971. A critical comparison of mercury porosimetry and capillary condensation pore size distributions of portland cement pastes. Cem. Conc. Res. 1: 531-545.

12. Diamond, S. 1972. A reply to the discussion by J. J. Beaudoin. Cem. Conc. Res. 2: 148-151.

13. Diamond, S. and W. L. Dolch. 1972. Generalized log-normal distribution of pore sizes in hydrated cement paste. J. Colloid Interface Sci. 38: 234-244.

14. Frevel, L. K. and L. J. Kressley. 1963. Modifications in mercury porosimetry. Anal. Chem. 35: 1492-1502.

15. Hill, R. D. 1960. A study of pore-size distribution. Trans. Brit. Ceram. Soc. 59: 198-212.

16. Kruyer, S. 1958. The penetration of mercury and capillary condensation in packed spheres. Trans. Farad. Soc. 54: 1758-1767.

17. Lea, F. M. 1970. The chemistry of cement and concrete. Edward Arnold Publishers Ltd., London.

18. Lee, J. A. and W. C. Maskell. 1973. Correction factors involved in mercury porosimetry. Powder Tech. 7: 259-262.

19. Mayer, R. P. and R. A. Stowe. 1965. Mercury porosimetry - breakthrough pressure for penetration between packed spheres. J. Colloid Sci. 20: 893-911.

20. Mayer, R. P. and R. A. Stowe. 1966. Mercury porosimetry: Filling of torroidal void volume following breakthrough between packed spheres. J. Phys. Chem. 70: 3867-3873.

21. Mikhail, R. Sh., D. H. Turk, and S. Brunauer. 1975. Dimensions of the average pore, the number of pores, and the surface area of hardened portland cement paste. Cem. Conc. Res. 5: 433-442.

22. Powers, T. C. 1960. Physical properties of cement paste and concrete. Proc. 4th Int. Symp. on the Chemistry of Cement. Nat. Bureau of Standards Monograph 2: 577-613.

23. Quynn, R. G. 1963. Internal volume in fibers. Text. Res. J. 33: 21-34.

24. Ritter, H. L. and L. C. Drake. 1945. Pore size distribution in porous materials. Ind. Eng. Chem. Anal. Ed. 17: 782-791.

25. Rootare, H. M. 1968. A short literature review of mercury porosimetry as a method of measuring pore-size distributions in porous materials, and a discussion of possible sources of error in this method. American Instrument Co. Bulletin 2330.

26. Sellevold, E. J. 1974. Mercury porosimetry of hardened cement paste cured or stored at 97°C. Cem. Conc. Res. 4: 399-404.

27. Taylor, H. F. W. 1964. The chemistry of cements. Vol. 1. Academic Press, New York.

28. Troxell, G. E., H. E. Davis, and J. W. Kelly. 1968. Composition and properties of concrete. McGraw-Hill Book Co., New York.

29. VanVlack, L. H. 1971. Materials science for engineers. Addison-Wesley Publishing Co., Reading.

30. Washburn, E. W. 1921. Note on a method of determining the distribution of pore sizes in a porous material. Proc. Nat. Acad. Sci. 7: 115-116.

31. Watson, A., J. O. May, and B. Butterworth. 1957. Studies of pore size distribution. Trans. Brit. Ceram. Soc. 56: 38-52.

32. Weast, C. R., ed. 1965. Handbook of chemistry and physics. 46th ed. The Chemical Rubber Co., Cleveland.

33. Winslow, D. N. and S. Diamond. 1970. A mercury porosimetry study of the evolution of porosity in portland cement. J. Mater. 5: 564-585.

34. Winslow, D. N. and S. Diamond. 1974. Specific surface of hardened cement paste as determined by small-angle X-ray scattering. J. Am. Ceram. Soc. 57(5): 193-197.

ACKNOWLEDGMENTS

The author was supported by the Turkish Ministry of Education during this study. The experimental work was supported by the Engineering Research Institute and the Department of Civil Engineering of Iowa State University.

The author wishes to express his gratitude to his major professors, Dr. T. Demirel and Dr. R. A. Lohnes, not only for their invaluable guidance, encouragement, assistance and friendship during this study, but also for their concern in providing the support needed for the experimental work.

The enthusiasm shown by the members of the advisory committee, namely, Dr. R. T. Greer, Dr. D. Y. Lee, Dr. T. D. McGee and Dr. T. D. Wheelock, is also gratefully acknowledged.